Demasi, L., Ashenafi, Y., Cavallaro, R., and Santarpia, E. (2015). Generalized unified formulation shell element for functionally graded variable-stiffness composite laminates and aeroelastic applications. Composite Structures, 131, 501-515

DOI: https://doi.org/10.1016/j.compstruct.2015.05.022

Generalized Unified Formulation Shell Element for Functionally Graded Variable-Stiffness Composite Laminates and Aeroelastic Applications

Luciano Demasi [a,*]

[a] *Associate Professor, Department of Aerospace Engineering, San Diego State University*

Yonas Ashenafi [b]

[b] *Master Student, Department of Aerospace Engineering, San Diego State University, also Stress Engineer, UTC Aerospace Systems, San Diego, California*

Rauno Cavallaro [d]

[c] *PhD Candidate, Department of Aerospace Engineering, San Diego State University and Department of Structural Engineering, University of California San Diego*

Enrico Santarpia [d]

[d] *PhD Candidate, Department of Aerospace Engineering, San Diego State University and Department of Structural Engineering, University of California San Diego*

Abstract

Composite materials have been extensively used in engineering thanks to their lightweight, superior mechanical performances and possibility to tailor the structural behavior, increasing the available design space. Variable Angle Tow (VAT) structures exploits this advantage by adopting a curvilinear patterns for the fibers constituting the lamina.

This work, for the first time, extends the Generalized Unified Formulation (GUF) to the case of fourth-order triangular shell elements and VAT composites. Functionally graded material properties in both the thickness and in-plane directions are also possible. The finite element has been formulated with layers of variable thickness with respect to the in-plane coordinates.

GUF is a very versatile tool for the analysis of Variable Stiffness Composite Laminates (VSCLs): it is possible to select generic element coordinate systems and define different types of axiomatic descriptions (Equivalent Single Layer, Layer Wise, and Zig-Zag enhanced formulations) and orders of the thickness expansions. Each displacement is independently treated from the others. All the infinite number of theories that can be generated with GUF are obtained by expanding six theory-invariant kernels (formally identical for all the elements), allowing a very general implementation. Finally, the possibility of tailoring the theory/order to increase the accuracy in desired directions makes the GUF VAT capability a very powerful tool for the design of aerospace structures.

Key words: Generalized Unified Formulation, Variable Angle Tows, Tailorable Directional Accuracy, Multi-Theory Framework.

1 Introduction

COMPOSITE structures have been used in several aerospace engineering applications due to their lightweight and great strength. Moreover, composites offer the possibility of customizing the mechanical behavior with freedom in the choice of materials for matrix and fibers, number of layers, and stacking sequence. Application of such design freedom could be in the aeroelastic tailoring (see ref. [67]) inducing for example a bending-torsion coupling that could reduce the likelihood of having instabilities such as divergence.

Traditional straight fiber composites, *Constant Stiffness Composite Laminates* (CSCLs), can be further enhanced by allowing the fiber orientation to change in space. This increases the design space towards more efficient structures. For example, aircraft fuselage presents some regions dominated by bending adjacent to areas in which shear deformation mainly affects the response (see [3]). In that case, the fibers would best be aligned to a certain direction to optimize the bending response; however, the fibers should be placed at 45 degrees to have a more efficient design in respect to the shear. A method to achieve this variability in stiffness properties and tailor the behavior of the structure is to use *Variable Stiffness Composite Laminates* (VSCLs) obtained with *curvilinear fibers' paths* (another term used in this work is *Variable Angle Tow* (VAT) composites).

VAT composites have been explored for the last few decades. Refs. [38] showed that with curvilinear fibers it was possible to improve stress concentration around holes. This was accomplished by arranging the fibers in the direction of critical load paths.

* Corresponding author
Email address: ldemasi@mail.sdsu.edu (Luciano Demasi).

Ref. [43] analyzed the postbuckling progressive damage behavior of Variable Stiffness Composite Laminates. The importance of taking into account the residual thermal stress resulting from the curing process was emphasized. It was also showed that VSCLs demonstrate capacity for load redistribution: the curvilinear fiber panels can redirect load fluxes from the central regions to their stiffer edges. The buckling load is then increased as a consequence.

Tow-steered laminate exhibiting bistability have been studied for a trailing edge flap application or where it is necessary to sustain significant changes in shape without the need for a continuous power supply. Ref. [53] discussed how to accurately predict the cured shapes of tow-steered laminates that are intended to be *bistable*.

Ref. [41] introduced a fiber placement technique (Continuous Tow Shearing) for the manufacturing of VAT composites with tailored fiber paths.

Prebuckling analysis of anisotropic VAT plates using Airy's stress function was presented in ref. [56].

Ref. [23] addressed the problem of *impact and compression after impact* of VSCLs with emphasis on the interaction between fiber orientations, matrix-crack and delaminations. The simulations were carried out using an explicit finite element analysis.

Aeroelastic behavior of a rectangular unswept composite wing combined with modified strip theory aerodynamics was studied in ref. [64]. Flutter, divergence, and gust loads were investigated, showning that the speed of instability occurrence could be influenced, both positively and negatively, by changing the fiber angle along the wingspan. It was also observed that VAT laminates allowed improved design compared to traditional unidirectional composite laminates.

Ref. [73] introduced a semi-analytical formulation based on a variational approach and Rayleigh-Ritz method to solve the postbuckling problem of VAT plates. The advantage of using variable stiffness for *enhanced postbuckling performance* of composite laminates was demonstrated.

Ref. [57] studied the problem of *tailoring* the in-plane tow path of VAT composite plates for improved postbuckling resistance.

Ref. [72] investigated the structural performance of axially compressed tow-steered shells. Both experimental and computational (finite element analysis) approaches were adopted. Prebuckling stiffness and buckling loads were estimated.

An optimization strategy (based on a genetic algorithm) for the design of *postbuckling* behavior of VAT composite laminates under axial compression was shown in ref. [74].

Ref. [3] introduced a Third Order Shear Deformation Theory (p-version Finite Element approach) with geometric nonlinear effects. Studies on the curvilinear fibers showed the possibility of reducing deflections and stresses under some static loadings. VSCLs led to changes in the stresses altering the position of maximum stress at the plate. It was concluded that this modification could be exploited to improve damage resistance in particular applications.

In Ref. [76] VSCLs were analyzed with a p-version Layer Wise finite element approach. Unsymmetric laminates with curvilinear fibers were analyzed with just one element. Moderately large deflection model (von Kármán strain-displacement relationships) was assumed. The Layer Wise displacement field assumed linear variation in the thickness for the in-plane displacements and constant transverse displacement. Different behavior was found in several unsymmetric laminates: a plate with relatively large displacement was actually stiffer in the nonlinear regime, showing the importance of taking into account geometric nonlinearities.

Ref. [2] presented a Third-Order Shear Deformation Theory for VSCL rectangular plates. Geometric nonlinearities and damage under various static and dynamic loads (uniform, localized, sinusoidal, and impact) were analyzed.

Refs. [77] developed a Layer Wise model in which a First Order Shear Deformation Theory was adopted for each layer. Plates with classical straight-fiber and curvilinear layers were investigated. The curvilinear fibers were used between plies with straight fibers. It was concluded that one can still take advantage of the variable stiffness plates (e.g., redistribute the applied load in the plane [43]) by mixing constant stiffness with variable stiffness plies along the thickness.

Ref. [21] discussed manufacturing characteristics of Variable Angle Tow structures with particular attention on layup accuracy, and thickness variation. An experimental approach (layup tests) was adopted.

Ref. [68] highlighted the advantages of having fiber-reinforcement following curvilinear paths in space. The initial post-buckling response of variable-stiffness cylindrical panels was presented. The model aimed to get an efficient tool for optimization studies of variable-stiffness panels where stability represents a constraint.

Ref. [22] introduced a First Order Shear Deformation Theory for buckling analysis of *thick stiffened* Variable Angle Tow panels.

Ref. [37] investigated the stability of VAT panels. It was observed that the

Variable Angle Tows laminates manufactured with the Continuous Tow Shearing technique produce laminates with a flat profile on one side and a curved profile on the other. Variable thickness was then modeled. An equivalent single layer model, taking into account shear effects, was adopted. The 3D structure was simulated either as a cylindrical shell or a flat plate. It was argued that the buckling event of the variable angle tow with variable thickness was characterized more by a "shell-like" behavior rather than a "plate-like" behavior.

From the above discussion of literature, there is a vast body of work on curvilinear fibers showing the design advantages that can be exploited in increase of buckling load and reduction of stresses. Several models have been introduced with aim to efficient optimization of VAT panels/structures.

With the present effort, *the authors introduce the Generalized Unified Formulation (GUF) [26, 32, 27, 28, 29, 30, 31, 33] for VAT structures for the first time*.

GUF allows one to define an independent local element coordinate system and have different axiomatic models for the different displacement variables. This allows the user to have the design freedom and computational efficiency where actually required by the problem under investigation.

To provide a general background on the theoretical models developed for the analysis of composites (and in some cases for VAT structures as previously discussed), a brief overview on the various axiomatic formulations is provided next.

2 Axiomatic Formulations for the Analysis of Composite Structures

2.1 Background and Literature Study

It is well know that composites do not have the same behavior in all the directions. This is actually exploited in the practice but also constitutes a difficulty when a good model is sought. Classical Plate Theory (CPT) [42] is generally sufficient for metallic thin panels. When some of the assumptions made in its formulation are removed, the resulting theories can more efficiently capture behaviors typical of composite laminates (for example the Zig-Zag form of the displacements, see ref. [33]). Thus, people formulated First Order Shear Deformation Theory (FSDT) [60, 46]. FSDT was improved even more with the introduction of the so-called Higher Order Shear Deformation Theories (HSDTs) [65, 6, 39, 75, 51, 44, 45]. Some researchers modified HSDTs by adding the transverse strain effects (more details can be found in ref. [33]). This was achieved by adding additional terms in the thickness expansion of the transverse displacement u_z.

It is known that the interlaminar equilibrium of the transverse stresses and anisotropy of the mechanical properties along the thickness determines a discontinuity of the first displacement derivatives with respect to the thickness coordinate z ("Zig Zag form of the displacements", see refs. [5, 1, 40]). Following the historical reconstruction provided in ref. [17] and the discussions found in ref. [33], the Zig Zag theories can be subdivided into 3 major groups:

- Lekhnitskii Multilayered Theory (LMT)
- Ambartsumian Multilayered Theory (AMT)
- Reissner Multilayered Theory (RMT)

Particularly relevant is the contribution provided by Murakami who proposed in ref. [48] to take into account the Zig Zag effects by *enhancing* the corresponding displacement variable with a Zig Zag function denoted here as Murakami's Zig Zag Function (MZZF). Numerous applications [19, 24, 25, 30, 13, 12, 11, 62] of the concept of enhancing the displacement field with MZZF have been presented. This enhancement provides a significant improvement of the accuracy with a marginal increment of the computational cost with respect to the inexpensive (but less accurate) classical methods.

Recently researchers [63, 52, 4, 55, 66] adopted Zig Zag models to solve various problems involving bending analysis of functionally graded sandwich structures, laminated beams, and buckling calculations. The effectiveness of taking into account the displacements' slope discontinuity at the interfaces with Zig Zag models was proven.

For a detailed quasi-3D type of investigation a Layer Wise [20, 50, 58, 61, 59, 16, 15] description represents a valuable alternative to the computationally demanding Finite Element approaches based on solid elements.

It is very valuable to the engineers to have the possibility of tailoring the accuracy/computational cost to better simulate a new problem without implementing new finite element solvers/capabilities every time a new need arises. Several methods, able to provide a large number of theories with a unified approach, have been proposed in the literature (see for example the works of Batra and coauthors, refs. [6] and [54]). Particularly interesting is the formulation proposed by Todd Williams (refs. [69, 70, 71]) in which Equivalent-Single-Layer approaches and Layer-Wise ones coexist in the same theoretical framework. Another option, on which the present effort is based upon, is represented by the so-called Compact Notations (CNs) (see ref. [26] for more details). The idea behind CNs is to write the axiomatic expansions in indicial form, so that all the possible theories can be generated from theory-invariant

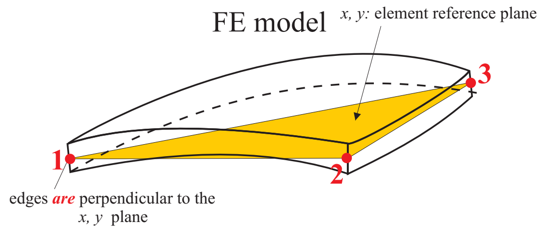

Fig. 1. Selection of the element reference plane.

kernels (also referred as nuclei). Carrera introduced this kind of representation for the modeling of structures. One of the earliest contributions is represented by ref. [14] (at that time the terminologies of Compact Notations and Carrera's Unified Formulation (CUF) were not adopted; only much later, in ref. [26] they were explicitly introduced and used since then). The displacement vectors were written using this formalism and the fundamental nuclei were 3×3 matrices (see [18]). Later the work was generalized by adopting the expansion at component level (Generalized Unified Formulation (GUF) [26, 27, 28, 29, 30, 31, 32, 33]) and so obtaining 1×1 kernels. In parallel, the group led by Carrera made significant contributions in other areas (multifield problems, functionally graded structures, advanced 1D-models with quasi-3D accuracy etc.) not discussed here for brevity.

This research extends the Generalized Unified Formulation to the case of Variable Angle Tow structures and fourth order triangular shell finite element.

The types of theories that can be generated with the GUF approach are the Advanced Higher Order Shear Deformation Theories (AHOSDTs), Zig-Zag Theories (ZZTs), Advanced Zig-Zag Theories (AZZTs), Layer Wise (LW) Theories, Partially Zig Zag Higher Order Shear Deformation Theories (PZ-ZHSDTs), Partially Zig Zag Advanced Higher Order Shear Deformation Theories (PZZAHSDTs), Partially Layer Wise Higher Order Shear Deformation Theories (PLHSDTs), Partially Layer Wise Advanced Higher Order Shear Deformation Theories (PLAHSDTs), Partially Layer Wise Zig Zag and Higher Order Shear Deformation Theories (PLZZHSDTs) and are extensively discussed in refs. [33] and [34].

3 Notations, Coordinate Systems at Element Level, and Transformations

Consider a portion of the structure (triangular element). With reference to Figure 1, all the edges in the undeformed continuum are assumed perpendicular to the reference plane identified as shown in Figure 1. The corner nodes 1, 2, and 3 are identified by a local numbering freely selected by the user. The notation and coordinate systems (see Figure 2) are now introduced. The

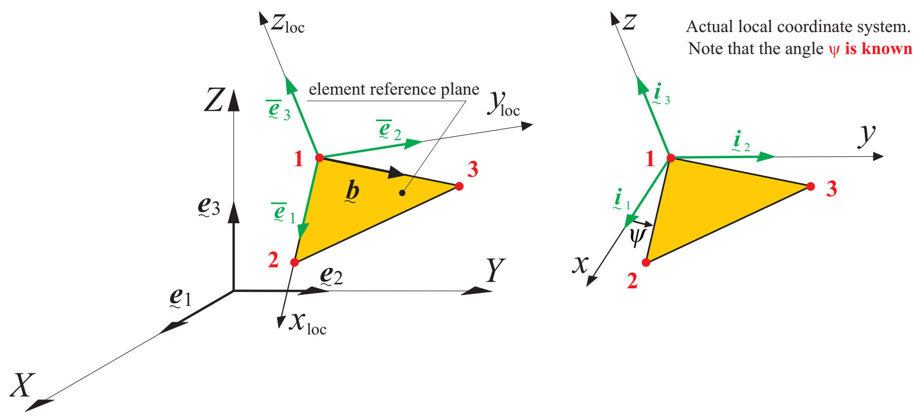

Fig. 2. Global and local coordinate systems, for a triangular element

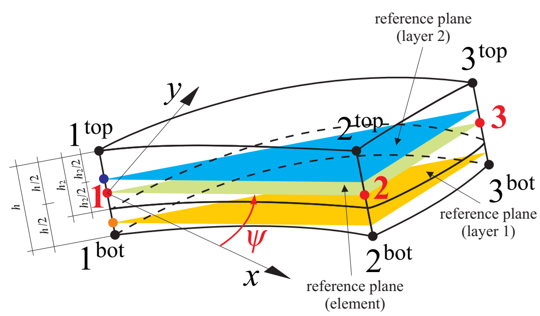

Fig. 3. Layer and element reference planes are parallel. Note that the layer thickness is not constant.

global axes are X, Y, Z. The corresponding unit vectors are indicated with $\underset{\sim}{e}_1$, $\underset{\sim}{e}_2$, and $\underset{\sim}{e}_3$. The auxiliary unit vectors $\underset{\sim}{\overline{e}}_1$, $\underset{\sim}{\overline{e}}_2$, and $\underset{\sim}{\overline{e}}_3$ are referred to an intermediate local coordinate system x_{loc}, y_{loc}, and z_{loc} (see Figure 2). This intermediate coordinate system has the x_{loc} connecting nodes 1 and 2 of the element.

The final unit vectors of the local coordinate system at *element level* are indicated with $\underset{\sim}{i}_1$, $\underset{\sim}{i}_2$, and $\underset{\sim}{i}_3$ respectively. x, y, and z are the actual *local coordinates* of the element under consideration. The local coordinate system is selected by the user. Thus, the angle ψ (see Figure 2) is assigned and known. Note that all the layers may have variables thicknesses. However, the *plate assumption* will be considered. Thus, all the coordinate systems at layer levels will be considered to be on parallel planes. That is, *all the layers will have parallel reference planes*. This is consistent with the assumption of flat element approximating a curved surface (see Figure 3). The angle ψ will then be the same for all the layers. Notice that the origin of the element coordinate system does not have to be necessarily on node 1. It can be anywhere even outside the element. However, the node 1 is selected for simplicity. After some simple algebra involving the rotation of coordinate systems, it is possible to relate the unit vectors of the local system with the ones of the global coordinate system:

$$\begin{aligned}
\underset{\sim}{\boldsymbol{i}}_1 &= a_{11}\underset{\sim}{\boldsymbol{e}}_1 + a_{12}\underset{\sim}{\boldsymbol{e}}_2 + a_{13}\underset{\sim}{\boldsymbol{e}}_3 \\
\underset{\sim}{\boldsymbol{i}}_2 &= a_{21}\underset{\sim}{\boldsymbol{e}}_1 + a_{22}\underset{\sim}{\boldsymbol{e}}_2 + a_{23}\underset{\sim}{\boldsymbol{e}}_3 \\
\underset{\sim}{\boldsymbol{i}}_3 &= a_{31}\underset{\sim}{\boldsymbol{e}}_1 + a_{32}\underset{\sim}{\boldsymbol{e}}_2 + a_{33}\underset{\sim}{\boldsymbol{e}}_3
\end{aligned} \tag{1}$$

where

$$\begin{aligned}
a_{11} &= \cos\psi\,\mathcal{A}_1 - \sin\psi\,\mathcal{B}_1 \quad & a_{21} &= \sin\psi\,\mathcal{A}_1 + \cos\psi\,\mathcal{B}_1 \quad & a_{31} &= \mathcal{C}_1 \\
a_{12} &= \cos\psi\,\mathcal{A}_2 - \sin\psi\,\mathcal{B}_2 \quad & a_{22} &= \sin\psi\,\mathcal{A}_2 + \cos\psi\,\mathcal{B}_2 \quad & a_{32} &= \mathcal{C}_2 \\
a_{13} &= \cos\psi\,\mathcal{A}_3 - \sin\psi\,\mathcal{B}_3 \quad & a_{23} &= \sin\psi\,\mathcal{A}_3 + \cos\psi\,\mathcal{B}_3 \quad & a_{33} &= \mathcal{C}_3
\end{aligned} \tag{2}$$

The explicit expressions of all the terms appearing in equation 2 are reported in Ref. [34].

4 Definition of the Fibers' Curvilinear Path at Layer and Element Levels

The proposed finite element presents a generic definition of the pattern defining the curvilinear fiber. This is achieved as follows.

Consider a user-selected *layer coordinate system* $\widehat{x}^k$, $\widehat{y}^k$ and $\widehat{z}^k$ with origin on a point on the layer reference plane (see Figure 3). This coordinate system is adopted to identify the fibers' paths. Note that each layer needs to have its own coordinate system so that general Variable Angle Tow multi-layer structures can be easily modeled. Given a triangular finite element, the curvilinear fibers' paths need to be provided. The user can select some points and *curve fitting* may be adopted to retrieve an analytical expression. From a practical point of view, one needs to provide the *"fundamental curve"* which is then replicated with translation in the element coordinate system (see Figure 4). The fundamental curve is conveniently defined in a different coordinate system ξ^k, η^k (see Figure 5) where Legendre polynomials can be defined. Let $\widehat{y}^k_{\max}$ be the *largest* $\widehat{y}^k$ coordinate (it can be negative). In the example of Figure 4 it corresponds to point 1. Similarly, it is possible to define $\widehat{y}^k_{\min}$ (in the example of Figure 4 it corresponds to point 2), $\widehat{x}^k_{\max}$ (in the example of Figure 4 it corresponds to point 3), and $\widehat{x}^k_{\min}$ (in the example of Figure 4 it corresponds to point 2). The new coordinate system is selected so that $\widehat{y}^k_{\max}$ corresponds to $\eta^k = 1$, $\widehat{y}^k_{\min}$ corresponds to $\eta^k = -1$, $\widehat{x}^k_{\max}$ corresponds to $\xi^k = 1$, and $\widehat{x}^k_{\min}$

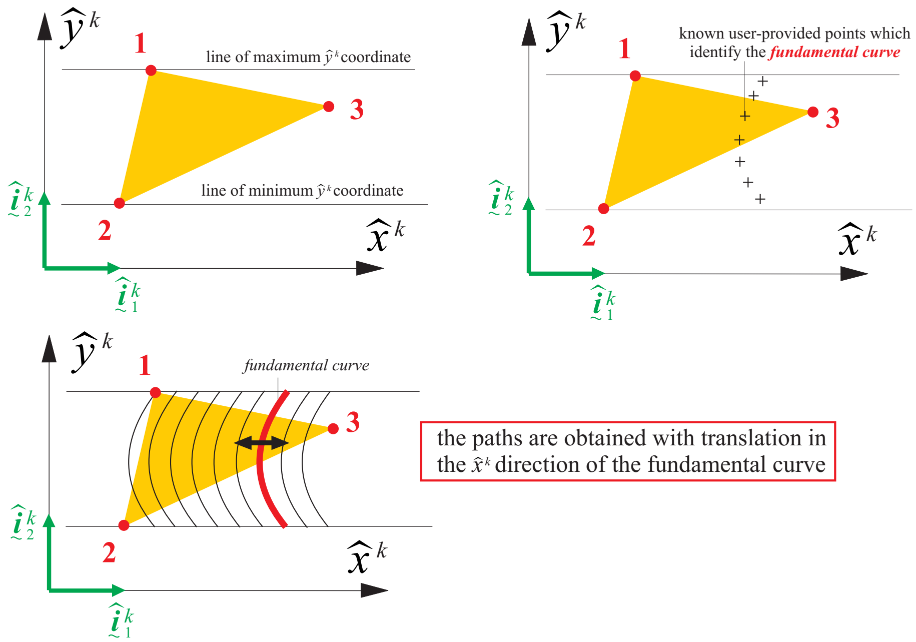

Fig. 4. Finite element and curvilinear fibers.

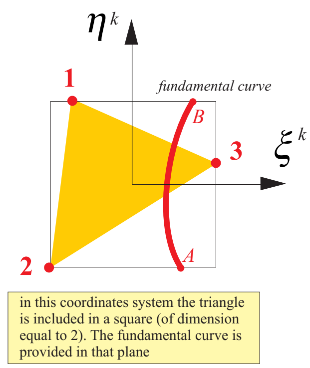

Fig. 5. Coordinate system in which the fundamental curve is defined.

corresponds to $\xi^k = -1$. The linear transformation is the following:

$$\begin{aligned}
\xi^k &= -\frac{\hat{x}^k_{\max} + \hat{x}^k_{\min}}{\hat{x}^k_{\max} - \hat{x}^k_{\min}} + \frac{2}{\hat{x}^k_{\max} - \hat{x}^k_{\min}}\hat{x}^k \\
\eta^k &= -\frac{\hat{y}^k_{\max} + \hat{y}^k_{\min}}{\hat{y}^k_{\max} - \hat{y}^k_{\min}} + \frac{2}{\hat{y}^k_{\max} - \hat{y}^k_{\min}}\hat{y}^k
\end{aligned} \tag{3}$$

and the inverse transformation is

$$\begin{aligned}
\hat{x}^k &= \frac{\hat{x}^k_{\max} + \hat{x}^k_{\min}}{2} + \frac{\hat{x}^k_{\max} - \hat{x}^k_{\min}}{2}\xi^k \\
\hat{y}^k &= \frac{\hat{y}^k_{\max} + \hat{y}^k_{\min}}{2} + \frac{\hat{y}^k_{\max} - \hat{y}^k_{\min}}{2}\eta^k
\end{aligned} \tag{4}$$

Let μ^k be a *parameter* used to describe the fundamental curve in the ξ^k, η^k plane. It is selected to have point A (see Figure 5) when $\mu^k = -1$ and point B

when $\mu^k = +1$. Point A is *always* on the line of minimum $\widehat{y}^k$ coordinate. The fundamental curve is defined from the originally given points as a combination of Legendre polynomials $P_g^k\left(\mu^k\right)$ and $P_h^k\left(\mu^k\right)$ as follows:

$$\begin{aligned}
\xi^k\left(\mu^k\right) &= a_0^k P_0^k\left(\mu^k\right) + a_1^k P_1^k\left(\mu^k\right) + ... = a_q^k P_q^k\left(\mu^k\right) \qquad q = 0, 1, ..., Q \\
\eta^k\left(\mu^k\right) &= b_0^k P_0^k\left(\mu^k\right) + b_1^k P_1^k\left(\mu^k\right) + ... = b_h^k P_h^k\left(\mu^k\right) \qquad h = 0, 1, ..., H
\end{aligned} \tag{5}$$

(The reader should note that h also indicates the thickness. However, in this context h is used as an index) In the practice the coefficients of the Legendre polynomials are calculated with the collocation method. This is now briefly discussed for the variable ξ^k. Let's assume that $Q+1$ is the number of coefficients that need to be determined (for example, if $Q = 3$ it means that maximum polynomial included is the cubic one and so 4 coefficients need to be determined). $\xi^k\left(\mu^k\right)$ is then calculated *at the zeros* of the Legendre polynomial $Q+1$.

Each evaluation of $\xi^k\left(\mu^k\right)$ at the i^{th} zero corresponds to an equation. Then a system of equations is determined and the coefficients a_q^k found.

After collocation, the coefficients a_q^k and b_h^k are known. Using equations 4 and 5 the parametric representation of the fundamental curve becomes:

$$\begin{aligned}
\widehat{x}_f^k &= \frac{\widehat{x}_{\max}^k + x_{\min}^k}{2} + \frac{\widehat{x}_{\max}^k - \widehat{x}_{\min}^k}{2}\, a_q^k P_q^k\left(\mu^k\right) \\
\widehat{y}_f^k &= \frac{\widehat{y}_{\max}^k + \widehat{y}_{\min}^k}{2} + \frac{\widehat{y}_{\max}^k - \widehat{y}_{\min}^k}{2}\, b_h^k P_h^k\left(\mu^k\right)
\end{aligned} \tag{6}$$

The subscript f has been used to clearly indicate that the quantities are referred to the fundamental one.

All the other curves describing the fibers patterns (see Figure 4) are obtained from the fundamental curve by a rigid translation in the $\widehat{x}^k$ direction. Let $\widehat{x}_c^k$, $\widehat{y}_c^k$ be the coordinates of a point on one of these curves. From equation 6 it is immediately deduced:

$$\begin{aligned}
\widehat{x}_c^k\left(\mu^k\right) &= \widehat{x}_f^k\left(\mu^k\right) + d_c^k = \frac{\widehat{x}_{\max}^k + \widehat{x}_{\min}^k}{2} + \frac{\widehat{x}_{\max}^k - \widehat{x}_{\min}^k}{2}\, a_q^k P_q^k\left(\mu^k\right) + d_c^k \\
\widehat{y}_c^k\left(\mu^k\right) &= \widehat{y}_f^k\left(\mu^k\right) = \frac{\widehat{y}_{\max}^k + \widehat{y}_{\min}^k}{2} + \frac{\widehat{y}_{\max}^k - \widehat{y}_{\min}^k}{2}\, b_h^k P_h^k\left(\mu^k\right)
\end{aligned} \tag{7}$$

where d_c^k is a constant and represents the "distance", in the $\widehat{x}^k$ direction, of the curve from the fundamental one.

One important quantity that needs to be derived is the local angle[1] ϑ^k (see

[1] In the literature the angle is expressed as a value between -90 and $+90$ and this

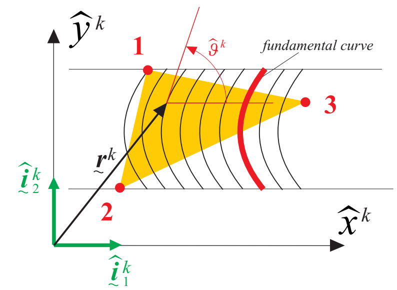

Fig. 6. Local fiber orientation angle.

Figures 6 and 7) at a given location identified by coordinates $\widehat{x}^k, \widehat{y}^k$. That point is on a curve which has expression of the type shown in equation 7:

$$\begin{aligned}\widehat{x}^k\left(\mu^k\right) &= \frac{\widehat{x}^k_{\max}+\widehat{x}^k_{\min}}{2}+\frac{\widehat{x}^k_{\max}-\widehat{x}^k_{\min}}{2}\,a_q^k P_q^k\left(\mu^k\right)+d^k \\ \widehat{y}^k\left(\mu^k\right) &= \frac{\widehat{y}^k_{\max}+\widehat{y}^k_{\min}}{2}+\frac{\widehat{y}^k_{\max}-\widehat{y}^k_{\min}}{2}\,b_h^k P_h^k\left(\mu^k\right)\end{aligned} \tag{8}$$

where d^k is a positive or negative constant which has similar meaning of d_c^k earlier discussed. In the practical problem it is not actually relevant to know the value of d^k. The position vector $\boldsymbol{r}^k\left(\mu^k\right)$ (see Figure 6) is:

$$\underset{\sim}{\boldsymbol{r}}^k\left(\mu^k\right)=\widehat{x}^k\left(\mu^k\right)\underset{\sim}{\widehat{\boldsymbol{i}}}{}_1^k+\widehat{y}^k\left(\mu^k\right)\underset{\sim}{\widehat{\boldsymbol{i}}}{}_2^k \tag{9}$$

The unit tangent vector $\underset{\sim}{\boldsymbol{v}}^k$ (see Figure 7) is:

$$\underset{\sim}{\boldsymbol{v}}^k\left(\mu^k\right)=\frac{\dfrac{\mathrm{d}\underset{\sim}{\boldsymbol{r}}^k\left(\mu^k\right)}{\mathrm{d}\mu^k}}{\left|\dfrac{\mathrm{d}\underset{\sim}{\boldsymbol{r}}^k\left(\mu^k\right)}{\mathrm{d}\mu^k}\right|}=\frac{\dfrac{\mathrm{d}\widehat{x}^k\left(\mu\right)}{\mathrm{d}\mu^k}\underset{\sim}{\widehat{\boldsymbol{i}}}{}_1^k+\dfrac{\mathrm{d}\widehat{y}^k\left(\mu^k\right)}{\mathrm{d}\mu^k}\underset{\sim}{\widehat{\boldsymbol{i}}}{}_2^k}{\sqrt{\left(\dfrac{\mathrm{d}\widehat{x}^k\left(\mu^k\right)}{\mathrm{d}\mu^k}\right)^2+\left(\dfrac{\mathrm{d}\widehat{y}^k\left(\mu^k\right)}{\mathrm{d}\mu^k}\right)^2}} \tag{10}$$

where the derivatives are calculated from equation 8:

$$\begin{aligned}\frac{\mathrm{d}\widehat{x}^k\left(\mu^k\right)}{\mathrm{d}\mu^k} &= \frac{\widehat{x}^k_{\max}-\widehat{x}^k_{\min}}{2}\,a_q^k P_q'^k\left(\mu^k\right) \\ \frac{\mathrm{d}\widehat{y}^k\left(\mu^k\right)}{\mathrm{d}\mu^k} &= \frac{\widehat{y}^k_{\max}-\widehat{y}^k_{\min}}{2}\,b_h^k P_h'^k\left(\mu^k\right)\end{aligned} \tag{11}$$

In reality, the layer coordinate system $\widehat{x}^k$ and $\widehat{y}^k$ is not used to define the fibers' angles. The element coordinate system x, y needs to be adopted (see

---

is the form that will be used to present the results. However, in this theoretical formulation the angle is selected to vary from 0 to 360 for convenience.

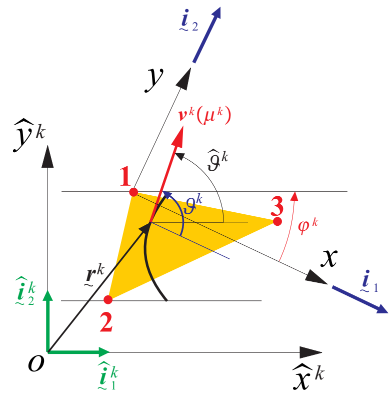

Fig. 7. Element coordinate system and element's fiber coordinate system.

Figure 7). A transformation of coordinates is in place:

$$
\begin{aligned}
\widehat{x}^{\,k} &= +\left(x - x_o\right)\cos\varphi^{\,k} + \left(y - y_o\right)\sin\varphi^{\,k} \\
\widehat{y}^{\,k} &= -\left(x - x_o\right)\sin\varphi^{\,k} + \left(y - y_o\right)\cos\varphi^{\,k}
\end{aligned}
\tag{12}
$$

where x_o and y_o are the coordinates (x, y coordinate system) of the origin of the cartesian frame $\widehat{x}^{\,k}, \widehat{y}^{\,k}$ (in the case of Figure 7 x_o is positive whereas y_o is negative).

The angle $\varphi^{\,k}$ indicates a counterclockwise (i.e., positive rotation if consistent with the element thickness coordinate z according to the right hand rule) rotation required to make the local coordinates x, y parallel to $\widehat{x}^{\,k}, \widehat{y}^{\,k}$. ($\varphi^{\,k}$ is defined in Figure 7). $\varphi^{\,k}$ is an input provided for each element.

The inverse of equation 12 is the following:

$$
\begin{aligned}
x &= \left(\widehat{x}^{\,k} - \widehat{x}_1^k\right)\cos\varphi^{\,k} - \left(\widehat{y}^{\,k} - \widehat{y}_1^k\right)\sin\varphi^{\,k} \\
y &= \left(\widehat{x}^{\,k} - \widehat{x}_1^k\right)\sin\varphi^{\,k} + \left(\widehat{y}^{\,k} - \widehat{y}_1^k\right)\cos\varphi^{\,k}
\end{aligned}
\tag{13}
$$

Equation 12 can be used to obtain the transformation of basis (see Figure 7 for a representation of the unit vectors):

$$
\begin{aligned}
\widehat{\underset{\sim}{\boldsymbol{i}}}{}_1^k &= +\cos\varphi^{\,k}\,\underset{\sim}{\boldsymbol{i}}_1 + \sin\varphi^{\,k}\,\underset{\sim}{\boldsymbol{i}}_2 \\
\widehat{\underset{\sim}{\boldsymbol{i}}}{}_2^k &= -\sin\varphi^{\,k}\,\underset{\sim}{\boldsymbol{i}}_1 + \cos\varphi^{\,k}\,\underset{\sim}{\boldsymbol{i}}_2
\end{aligned}
\tag{14}
$$

and so it is now possible to calculate the trigonometric functions necessary to rotate the stiffness tensor (see equation 10 and consider equation 14):

$$\begin{aligned}
\left[\cos\vartheta^{k}\right]\left(\mu^{k}\right) = \underset{\sim}{\boldsymbol{v}}^{k}\left(\mu^{k}\right) \bullet \underset{\sim}{\boldsymbol{i}}_1 = \frac{\dfrac{\mathrm{d}\widehat{x}^{k}\left(\mu^{k}\right)}{\mathrm{d}\mu^{k}}\cos\varphi^{k} - \dfrac{\mathrm{d}\widehat{y}^{k}\left(\mu^{k}\right)}{\mathrm{d}\mu^{k}}\sin\varphi^{k}}{\sqrt{\left(\dfrac{\mathrm{d}\widehat{x}^{k}\left(\mu^{k}\right)}{\mathrm{d}\mu^{k}}\right)^2 + \left(\dfrac{\mathrm{d}\widehat{y}^{k}\left(\mu^{k}\right)}{\mathrm{d}\mu^{k}}\right)^2}} \\
\left[\sin\vartheta^{k}\right]\left(\mu^{k}\right) = \underset{\sim}{\boldsymbol{v}}^{k}\left(\mu^{k}\right) \bullet \underset{\sim}{\boldsymbol{i}}_2 = \frac{\dfrac{\mathrm{d}\widehat{x}^{k}\left(\mu^{k}\right)}{\mathrm{d}\mu^{k}}\sin\varphi^{k} + \dfrac{\mathrm{d}\widehat{y}^{k}\left(\mu^{k}\right)}{\mathrm{d}\mu^{k}}\cos\varphi^{k}}{\sqrt{\left(\dfrac{\mathrm{d}\widehat{x}^{k}\left(\mu^{k}\right)}{\mathrm{d}\mu^{k}}\right)^2 + \left(\dfrac{\mathrm{d}\widehat{y}^{k}\left(\mu^{k}\right)}{\mathrm{d}\mu^{k}}\right)^2}}
\end{aligned} \tag{15}$$

To calculate the stiffness matrix, it is necessary to evaluate the different quantities at the *Gauss points*. Let x_g and y_g be the coordinates of one of the elements's Gauss points (the element local coordinate system is considered). The trigonometric functions $\left[\sin\vartheta^{k}\right]\left(\mu^{k}\right)$ and $\left[\cos\vartheta^{k}\right]\left(\mu^{k}\right)$, expressed in equation 15, need to be found at each Gauss point. To achieve this, the corresponding parameter $\mu^{k} \equiv \mu_g^{k}$ has to be identified so that equation 11 and then equation 15 can be used. This is accomplished as discussed in Ref. [34].

5 Formulation of In-plane and Out-of-plane Functionally Graded Properties

The present shell formulation is made of several triangular plate elements. The geometric interfaces between layers are assumed to be a function provided by the user and can be non-planar surfaces. We know discuss the case of a generic layer k.

It should be noted that the coordinate system $\widehat{x}^{k}, \widehat{y}^{k}$ is not the local coordinate system x, y used to define the finite element matrices. This is done *to allow a very general placement of the fiber patterns*. The choice of the local coordinate system x, y is related to the orders of expansion, type of theory etc. which are used in the Generalized Unified Formulation framework. This approach provides great versatility and generality of the finite element implementation because the user can decide to increase the accuracy of the description in any desired direction (for example the local y direction in one element and the local x direction in another element).

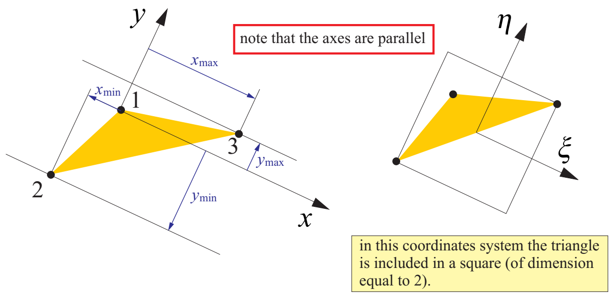

Fig. 8. Element coordinate system used to define the thickness variation along the plate. Note that a single coordinate system is used for the entire plate.

5.1 Element's Variable Thickness

Modeling the variability of thickness may be relevant in Variable Angle Tow Composite Laminates (see Figs. 1 and 4 of ref. [37]). How this is accomplished in the present computational architecture is discussed next.

The bottom surface of layer k is indicated as z_{bot_k}. The top surface is indicated as z_{top_k}.These surfaces are both functions of x, y if the element thickness is not constant. z_{bot_k} and z_{top_k} are measured from the reference coordinate system of the entire plate (not the layer's one: see Figure 3 for a pictorial representation of the element reference plane). These functions are provided in the coordinate system reported in Figure 8. The layer interfaces are expressed as a function of products of Legendre polynomials of both coordinates ξ and η:

$$
\begin{aligned}
z_{\mathrm{top}_k}(\xi,\eta) &= a_{\tau_{z_{\mathrm{top}_k}}} P_{\tau_{z_{\mathrm{top}_k}}}(\xi) \cdot a_{s_{z_{\mathrm{top}_k}}} P_{s_{z_{\mathrm{top}_k}}}(\eta) \\
z_{\mathrm{bot}_k}(\xi,\eta) &= a_{\tau_{z_{\mathrm{bot}_k}}} P_{\tau_{z_{\mathrm{bot}_k}}}(\xi) \cdot a_{s_{z_{\mathrm{bot}_k}}} P_{s_{z_{\mathrm{bot}_k}}}(\eta)
\end{aligned}
\tag{16}
$$

where

$$
\begin{aligned}
\tau_{z_{\mathrm{top}_k}} &= 0, 1, ..., N_\xi^{z_{\mathrm{top}_k}} \qquad & s_{z_{\mathrm{top}_k}} &= 0, 1, ..., N_\eta^{z_{\mathrm{top}_k}} \\
\tau_{z_{\mathrm{bot}_k}} &= 0, 1, ..., N_\xi^{z_{\mathrm{bot}_k}} \qquad & s_{z_{\mathrm{bot}_k}} &= 0, 1, ..., N_\eta^{z_{\mathrm{bot}_k}}
\end{aligned}
\tag{17}
$$

$N_\xi^{z_{\mathrm{top}_k}}$ is the degree of the Legendre polynomial used to express the functional dependance of z_{top_k} with respect to ξ, $N_\eta^{z_{\mathrm{top}_k}}$ is the degree of the Legendre polynomial used to express the functional dependance of z_{top_k} with respect to η; $N_\xi^{z_{\mathrm{bot}_k}}$ is the degree of the Legendre polynomial used to express the functional dependance of z_{bot_k} with respect to ξ, $N_\eta^{z_{\mathrm{bot}_k}}$ is the degree of the Legendre polynomial used to express the functional dependance of z_{bot_k} with respect to η. Due to the mapping shown in Figure 8, equation 16 can be

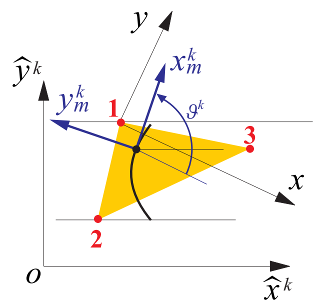

Fig. 9. Material coordinate system at a given location on a generic curvilinear fiber.

formally written in the physical coordinate system:

$$
\begin{aligned}
z_{\text{top}_k}(x,y) &= a_{\tau_{z_{\text{top}_k}}} P_{\tau_{z_{\text{top}_k}}}(x) \cdot a_{s_{z_{\text{top}_k}}} P_{s_{z_{\text{top}_k}}}(y) \\
z_{\text{bot}_k}(x,y) &= a_{\tau_{z_{\text{bot}_k}}} P_{\tau_{z_{\text{bot}_k}}}(x) \cdot a_{s_{z_{\text{bot}_k}}} P_{s_{z_{\text{bot}_k}}}(y)
\end{aligned}
\tag{18}
$$

Since the geometry of the multilayer structure made of layers with variable thickness is known, the coefficients of the expansion in equation 18 are provided by the user (preprocessing phase).

5.2 Element's Variable Material Properties in both In-plane and Out-of-plane Directions

The material is assumed *orthotropic* in its material coordinate system x_m^k, y_m^k, and z_m^k which changes point by point according to Figure 9. At any point the material coordinate system has one axis (x_m^k) tangent to the curve representing the curvilinear path at that point, another axis (y_m^k) is perpendicular to the first one and parallel to the reference plane. The third axis z_m follows the right hand rule and is directed along the z direction.

The quantities that need to be *point-by-point* defined are the Young moduli E_{11}^k, E_{22}^k, and E_{33}^k, the shear moduli G_{12}^k, G_{13}^k, and G_{23}^k, and Poisson's ratios υ_{12}^k, υ_{13}^k, and υ_{23}^k. For example, E_{11}^k is the elastic modulus in the x_m^k direction. Using the same logic that led to equation 18 and adopting Legendre polynomials in the thickness direction it is possible to write the explicit form of $G_{12}^k\left(x,y,z^k\right)$ as follows (details for the other material properties are reported in Appendix A of ref. [34]):

$$
G_{12}^k\left(x,y,z^k\right) = a_{\tau_{G_{12}^k}} P_{\tau_{G_{12}^k}}(x) \cdot a_{s_{G_{12}^k}} P_{s_{G_{12}^k}}(y) \cdot a_{r_{G_{12}^k}} P_{r_{G_{12}^k}}\left(z^k\right) \tag{19}
$$

where, for example, it is

$$
\tau_{G_{12}^k} = 0, 1, ..., N_\xi^{G_{12}^k}
$$

and $N_{\xi}^{G_{12}^{k}}$ indicates the order of the Legendre polynomial. Note that the functionally graded properties have to be provided layer by layer.

In the *material coordinate system* x_m^k, y_m^k, and z_m^k, Hooke's coefficients are calculated with the formulas reported in Ref. [34].

6 The Generalized Unified Formulation (GUF)

With GUF the variables are expanded in the thickness direction with an axiomatic approach. The following features are typical of the Generalized Unified Formulation for a displacement-based computational framework (i.e., the Principal of Virtual Displacements, PVD, is used to derive the governing equations):

- Given an *element* coordinate system x, y, z, a different type of representation is possible for each displacement component. For example, the displacement u_x in the x direction may be described with an *Equivalent Single Layer formulation*; the displacement u_y in the y direction my be axiomatically expanded with an Equivalent Single Layer approach but including Zig-Zag effects via Murakami's Zig-Zag Function (MZZF); the displacement u_z may be simulated with a Layer Wise (LW) theory.
- Different orders of expansions can be used for the different displacements. For example u_x may have a cubic expansion whereas u_z could have a parabolic dependence on the thickness coordinate.

The acronyms adopted to indicate the different theories are explained in refs. [33] and [34] and will not be reported here for brevity. It can be shown that the theory-invariant GUF writing of all the types of theories previously described can be reduced to the following expression:

$$\begin{aligned}
u_x^k &= {}^{x}F_{\alpha_{u_x}}\,{}^{x}N_i\,{}^{x}U_{\alpha_{u_x} i}^{k} \qquad \alpha_{u_x} = t, l, b; \quad l = 2, ..., N_{u_x}; \quad i = 1, 2, ..., N_n \\
u_y^k &= {}^{y}F_{\alpha_{u_y}}\,{}^{y}N_i\,{}^{y}U_{\alpha_{u_y} i}^{k} \qquad \alpha_{u_y} = t, m, b; \quad m = 2, ..., N_{u_y}; \quad i = 1, 2, ..., N_n \\
u_z^k &= {}^{z}F_{\alpha_{u_z}}\,{}^{z}N_i\,{}^{z}U_{\alpha_{u_z} i}^{k} \qquad \alpha_{u_z} = t, n, b; \quad n = 2, ..., N_{u_z}; \quad i = 1, 2, ..., N_n
\end{aligned} \tag{20}$$

6.1 *Governing Equations within GUF Formalism*

The governing equations are obtained by using the Principle of Virtual Displacements (see ref. [34] for details). The governing equations at *finite element* *level* read as follows:

$$\mathbf{K}_{UU} \cdot \mathbf{U} = \mathbf{P} \tag{21}$$

where $\mathbf{U}$ contains all the arrays of nodal displacements at element level and $\mathbf{P}$ contains all the arrays of nodal forces at element level. The explicit expressions for the arrays of unknown nodal displacements and known nodal loads (see equation 21) are:

$$\mathbf{U} = \begin{bmatrix} {}^{x}\mathbf{U} \\ {}^{y}\mathbf{U} \\ {}^{z}\mathbf{U} \end{bmatrix} \qquad \mathbf{P} = \begin{bmatrix} {}^{x}\mathbf{P} \\ {}^{y}\mathbf{P} \\ {}^{z}\mathbf{P} \end{bmatrix} \tag{22}$$

The finite element stiffness matrix $\mathbf{K}_{UU}$ (see equation 21) is:

$$\mathbf{K}_{UU} = \begin{bmatrix} \mathbf{K}_{u_x u_x} & \mathbf{K}_{u_x u_y} & \mathbf{K}_{u_x u_z} \\ \mathbf{K}_{u_x u_y}^T & \mathbf{K}_{u_y u_y} & \mathbf{K}_{u_y u_z} \\ \mathbf{K}_{u_x u_z}^T & \mathbf{K}_{u_y u_z}^T & \mathbf{K}_{u_z u_z} \end{bmatrix} \tag{23}$$

Note that the stiffness matrix of equation 23 is symmetric. The sub-matrices $\mathbf{K}_{u_x u_x}$, $\mathbf{K}_{u_y u_y}$, and $\mathbf{K}_{u_z u_z}$ are square symmetric matrices (in general of different sizes due to the fact that different representations and orders are possible for the displacements u_x, u_y, and u_z respectively). The partitions $\mathbf{K}_{u_x u_y}$, $\mathbf{K}_{u_x u_z}$, and $\mathbf{K}_{u_y u_z}$ are in general rectangular matrices.

6.2 *Theory-Invariant Arrays: Kernels of the Generalized Unified Formulation*

The governing equations (see equation 21) can be solved once $\mathbf{K}_{UU}$ is determined. Looking at equation 23, it appears clear that $\mathbf{K}_{UU}$ is built from the knowledge of *six* finite element matrices $\mathbf{K}_{u_x u_x}$, $\mathbf{K}_{u_x u_y}$, $\mathbf{K}_{u_x u_z}$, $\mathbf{K}_{u_y u_y}$, $\mathbf{K}_{u_y u_z}$, and $\mathbf{K}_{u_z u_z}$. This implies that the actual GUF's kernels required to generate the stiffness matrix are the following: $K_{u_x u_x}^{k\, \alpha_{u_x} \beta_{u_x} ij}$, $K_{u_x u_y}^{k\, \alpha_{u_y} \beta_{u_y} ij}$, $K_{u_x u_z}^{k\, \alpha_{u_x} \beta_{u_z} ij}$, $K_{u_y u_y}^{k\, \alpha_{u_y} \beta_{u_y} ij}$, $K_{u_y u_z}^{k\, \alpha_{u_y} \beta_{u_z} ij}$, and $K_{u_z u_z}^{k\, \alpha_{u_z} \beta_{u_z} ij}$. These matrices require evaluation of integrals over the volume of the layer (at element level). From a practical point of view the integral is split in an integral over the thickness and one over the element plane (indicated with Ω). Some examples of thickness integrals within GUF formalism are presented in Figure 10. z_{top_k} is the top layer z coordinate of the upper layer surface at a given location in the plane of element. z_{bot_k} has a similar meaning but is referred to the lower layer surface. After carrying out all integrations, the expressions for the six kernels of the Generalized Unified Formulation can be determined. Their formal writing is reported in Appendix

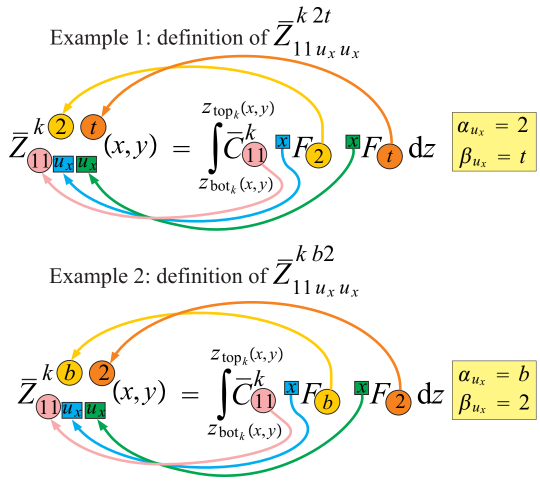

Fig. 10. Integrals along the thickness: definitions.

B of ref. [34]. For clarity, $K_{u_x\,u_y}^{k\,\alpha_{u_x}\beta_{u_y}ij}$ is reported below:

$$
\begin{aligned}
K_{u_x\,u_y}^{k\,\alpha_{u_x}\beta_{u_y}ij} = & \int_{\Omega} \overline{Z}_{12\,u_x\,u_y}^{k\,\alpha_{u_x}\beta_{u_y}}\, {}^{x}N_{i,x}\, {}^{y}N_{j,y} \mathrm{d}x\mathrm{d}y + \int_{\Omega} \overline{Z}_{16\,u_x\,u_y}^{k\,\alpha_{u_x}\beta_{u_y}}\, {}^{x}N_{i,x}\, {}^{y}N_{j,x} \mathrm{d}x\mathrm{d}y \\
& + \int_{\Omega} \overline{Z}_{26\,u_x\,u_y}^{k\,\alpha_{u_x}\beta_{u_y}}\, {}^{x}N_{i,y}\, {}^{y}N_{j,y} \mathrm{d}x\mathrm{d}y + \int_{\Omega} \overline{Z}_{66\,u_x\,u_y}^{k\,\alpha_{u_x}\beta_{u_y}}\, {}^{x}N_{i,y}\, {}^{y}N_{j,x} \mathrm{d}x\mathrm{d}y \\
& + \int_{\Omega} \overline{Z}_{45\,u_x\,u_y}^{k\,\alpha_{u_x,z}\,\beta_{u_y,z}}\, {}^{x}N_{i}\, {}^{y}N_{j} \mathrm{d}x\mathrm{d}y
\end{aligned} \tag{24}
$$

7 Interelement Boundary Conditions: the Penalty Method

Within this GUF extension to VAT structures, each element has different kinematics and types of theories referred to different local coordinate systems. Thus, the issue of combining (see refs. [8, 7, 9, 10]) different kinematic assumptions arises when the interlement compatibility needs to be imposed. In fact, due to the different discriminations among the adjacent elements, the classic assembling technique, which automatically assures the equality of the global displacements is not the optimal choice. This issue is overcome in this work by adopting the penalty method [36].

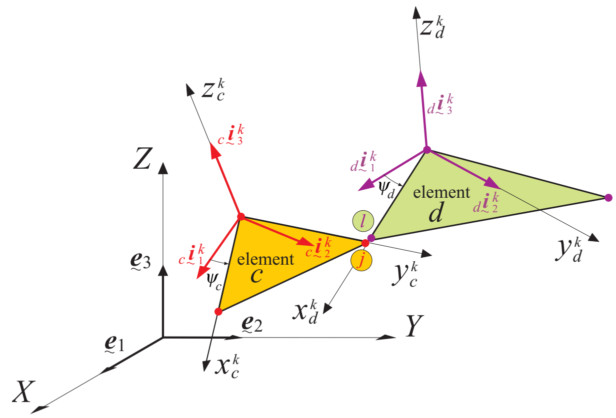

Fig. 11. The displacements of nodes j (element c) and l (element d) need to be imposed to be the same.

7.1 Displacements of the Linked Nodes

Within GUF formalism, the displacement in the *local* x^k direction [2] of a generic layer k is written as

$$u_x^k \left(x^k, y^k, z^k\right) = {}^{x}F^k_{\alpha_{u_x}} \left(z^k\right) {}^{x}N_i \left(x^k, y^k\right) {}^{x}U^k_{\alpha_{u_x} i} \tag{25}$$

In this formulation it is *assumed* that two adjacent layers (parts of elements denoted as element c and element d respectively) that have nodes j and l on the "same location" (which will be linked with springs) have the same thickness on that location. The thickness can be variable, but at the finite element nodes is assumed to be the same if the two elements are physically connected (see Figure 11). This is not really a limitation because the variability of the thickness can still be considered at element level.

Consequence of this assumption is that a point on layer k of element c will be linked to a point on layer k (note the same identity for the layer) of element d.

The displacement is evaluated in correspondence of a finite element node j of element c. All the element shape functions, except the one corresponding to node j, will be zero and the non-zero shape function takes the unitary value. Thus, it can be inferred (see equation 25) that:

$$_{c}u^k_{xj} = {}^{x}_{c}F^k_{\alpha_{\,c u_x}} \left(z^k_c\right) {}^{x}_{c}U^k_{\alpha_{\,c u_x} j} \tag{26}$$

where the subscript c has been added to emphasize that finite element c is considered. No summation is implied when the index c is repeated.

[2] Note that the in-plane coordinates x, y are the same for all the layers; thus, it is $x = x^k$ and $y = y^k$. For clarity of the presentation the superscript k is retained.

For the displacements in the other two local directions similar formula is valid:

$$ {}_c u^k_{yj} = {}^y_c F^k_{\alpha_{{}_c u_y}} \left(z^k_c \right) {}^y_c U^k_{\alpha_{{}_c u_y} j} \tag{27} $$

$$ {}_c u^k_{zj} = {}^z_c F^k_{\alpha_{{}_c u_z}} \left(z^k_c \right) {}^z_c U^k_{\alpha_{{}_c u_z} j} \tag{28} $$

The displacements must be understood in local coordinate system relative to element c (see Figure 11).

If ${}_c a^k_{mn}$ indicates the generic entry of the transformation matrix that transforms the components of a vector from global to local coordinate system (at layer level) of element c (similar logic can be used for element d), it is possible to refer equations 26-28 to the *global coordinate system* by multiplying the array representation of the displacement vector by the transpose of the transformation matrix. This means that the global displacements (indicated with ${}_c u^k_{Xj}$, ${}_c u^k_{Yj}$, ${}_c u^k_{Zj}$, imagined function of the *local* coordinates x^k_c, y^k_c, z^k_c) are the following:

$$
\begin{aligned}
{}_c u^k_{Xj} &= {}_c a^k_{11}\, {}_c u^k_{xj} + {}_c a^k_{21}\, {}_c u^k_{yj} + {}_c a^k_{31}\, {}_c u^k_{zj} \\
{}_c u^k_{Yj} &= {}_c a^k_{12}\, {}_c u^k_{xj} + {}_c a^k_{22}\, {}_c u^k_{yj} + {}_c a^k_{32}\, {}_c u^k_{zj} \\
{}_c u^k_{Zj} &= {}_c a^k_{13}\, {}_c u^k_{xj} + {}_c a^k_{23}\, {}_c u^k_{yj} + {}_c a^k_{33}\, {}_c u^k_{zj}
\end{aligned} \tag{29}
$$

or

$$
\begin{aligned}
{}_c u^k_{Xj} &= {}_c a^k_{11}\, {}^x_c F^k_{\alpha_{{}_c u_x}}\, {}^x_c U^k_{\alpha_{{}_c u_x} j} + {}_c a^k_{21}\, {}^y_c F^k_{\alpha_{{}_c u_y}}\, {}^y_c U^k_{\alpha_{{}_c u_y} j} + {}_c a^k_{31}\, {}^z_c F^k_{\alpha_{{}_c u_z}}\, {}^z_c U^k_{\alpha_{{}_c u_z} j} \\
{}_c u^k_{Yj} &= {}_c a^k_{12}\, {}^x_c F^k_{\alpha_{{}_c u_x}}\, {}^x_c U^k_{\alpha_{{}_c u_x} j} + {}_c a^k_{22}\, {}^y_c F^k_{\alpha_{{}_c u_y}}\, {}^y_c U^k_{\alpha_{{}_c u_y} j} + {}_c a^k_{32}\, {}^z_c F^k_{\alpha_{{}_c u_z}}\, {}^z_c U^k_{\alpha_{{}_c u_z} j} \\
{}_c u^k_{Zj} &= {}_c a^k_{13}\, {}^x_c F^k_{\alpha_{{}_c u_x}}\, {}^x_c U^k_{\alpha_{{}_c u_x} j} + {}_c a^k_{23}\, {}^y_c F^k_{\alpha_{{}_c u_y}}\, {}^y_c U^k_{\alpha_{{}_c u_y} j} + {}_c a^k_{33}\, {}^z_c F^k_{\alpha_{{}_c u_z}}\, {}^z_c U^k_{\alpha_{{}_c u_z} j}
\end{aligned} \tag{30}
$$

The superscript k is maintained even at global level to emphasize that layer k is considered.

Similar method is followed when a point, in correspondence of node l and element d is considered:

$$
\begin{aligned}
{}_d u^k_{Xl} &= {}_d a^k_{11}\, {}^x_d F^k_{\alpha_{{}_d u_x}}\, {}^x_d U^k_{\alpha_{{}_d u_x} l} + {}_d a^k_{21}\, {}^y_d F^k_{\alpha_{{}_d u_y}}\, {}^y_d U^k_{\alpha_{{}_d u_y} l} + {}_d a^k_{31}\, {}^z_d F^k_{\alpha_{{}_d u_z}}\, {}^z_d U^k_{\alpha_{{}_d u_z} l} \\
{}_d u^k_{Yl} &= {}_d a^k_{12}\, {}^x_d F^k_{\alpha_{{}_d u_x}}\, {}^x_d U^k_{\alpha_{{}_d u_x} l} + {}_d a^k_{22}\, {}^y_d F^k_{\alpha_{{}_d u_y}}\, {}^y_d U^k_{\alpha_{{}_d u_y} l} + {}_d a^k_{32}\, {}^z_d F^k_{\alpha_{{}_d u_z}}\, {}^z_d U^k_{\alpha_{{}_d u_z} l} \\
{}_d u^k_{Zl} &= {}_d a^k_{13}\, {}^x_d F^k_{\alpha_{{}_d u_x}}\, {}^x_d U^k_{\alpha_{{}_d u_x} l} + {}_d a^k_{23}\, {}^y_d F^k_{\alpha_{{}_d u_y}}\, {}^y_d U^k_{\alpha_{{}_d u_y} l} + {}_d a^k_{33}\, {}^z_d F^k_{\alpha_{{}_d u_z}}\, {}^z_d U^k_{\alpha_{{}_d u_z} l}
\end{aligned} \tag{31}
$$

7.2 Compatibility Enforced by Springs

The potential energy $\mathcal{U}_k$ of spring (of stiffness values $\mathcal{K}^k_X$, $\mathcal{K}^k_Y$, and $\mathcal{K}^k_Z$ respectively), written considering the displacements expressed in *global* coordinates (see ref. [35]), is:

$$\mathcal{U}_k = \frac{1}{2}\left[\begin{bmatrix} {}_c u^k_{Xj} \\ {}_c u^k_{Yj} \\ {}_c u^k_{Zj} \end{bmatrix} - \begin{bmatrix} {}_d u^k_{Xl} \\ {}_d u^k_{Yl} \\ {}_d u^k_{Zl} \end{bmatrix}\right]^T \begin{bmatrix} \mathcal{K}^k_X & 0 & 0 \\ 0 & \mathcal{K}^k_Y & 0 \\ 0 & 0 & \mathcal{K}^k_Z \end{bmatrix} \left[\begin{bmatrix} {}_c u^k_{Xj} \\ {}_c u^k_{Yj} \\ {}_c u^k_{Zj} \end{bmatrix} - \begin{bmatrix} {}_d u^k_{Xl} \\ {}_d u^k_{Yl} \\ {}_d u^k_{Zl} \end{bmatrix}\right] \tag{32}$$

Note that in equation 32 the indices j and l are not understood as variables: they indicate the nodes connected via springs as depicted in Figure 11.

Using equations 30 and 31 (which report the global displacements of the nodes that need to have the same displacements imposed via penalty method), equation 32 is rewritten as (no summation on repeated indices ll and jj is implied)

$$\begin{aligned} 2\mathcal{U}_k = & \\ & {}^x_c U^k_{\alpha_{{}_c u_x} j} \cdot K^{k\,\alpha\,{}_c u_x\,\beta\,{}_c u_x\,jj}_{{}_c u_x\,{}_c u_x} \cdot {}^x_c U^k_{\beta_{{}_c u_x} j} + {}^x_d U^k_{\alpha_{{}_d u_x} l} \cdot K^{k\,\alpha\,{}_d u_x\,\beta\,{}_c u_x\,lj}_{{}_d u_x\,{}_c u_x} \cdot {}^x_d U^k_{\beta_{{}_d u_x} l} + \\ & {}^x_c U^k_{\alpha_{{}_c u_x} j} \cdot K^{k\,\alpha\,{}_c u_x\,\beta\,{}_d u_x\,jl}_{{}_c u_x\,{}_d u_x} \cdot {}^x_d U^k_{\beta_{{}_d u_x} l} + {}^x_d U^k_{\alpha_{{}_d u_x} l} \cdot K^{k\,\alpha\,{}_d u_x\,\beta\,{}_d u_x\,ll}_{{}_d u_x\,{}_d u_x} \cdot {}^x_d U^k_{\beta_{{}_d u_x} l} + \text{other terms} \end{aligned} \tag{33}$$

where

$$\begin{aligned} K^{k\,\alpha\,{}_c u_x\,\beta\,{}_c u_x\,jj}_{{}_c u_x\,{}_c u_x} &= \left({}_c a^k_{11}\,{}_c a^k_{11}\mathcal{K}^k_X + {}_c a^k_{12}\,{}_c a^k_{12}\mathcal{K}^k_Y + {}_c a^k_{13}\,{}_c a^k_{13}\mathcal{K}^k_Z\right)\,{}^x_c F^k_{\alpha_{u_x}}\,{}^x_c F^k_{\beta_{u_x}} \\ K^{k\,\alpha\,{}_d u_x\,\beta\,{}_c u_x\,lj}_{{}_d u_x\,{}_c u_x} &= \left(-\,{}_c a^k_{11}\,{}_d a^k_{11}\mathcal{K}^k_X - {}_c a^k_{12}\,{}_d a^k_{12}\mathcal{K}^k_Y - {}_c a^k_{13}\,{}_d a^k_{13}\mathcal{K}^k_Z\right)\,{}^x_d F^k_{\alpha_{u_x}}\,{}^x_c F^k_{\beta_{u_x}} \\ K^{k\,\alpha\,{}_c u_x\,\beta\,{}_d u_x\,jl}_{{}_c u_x\,{}_d u_x} &= \left(-\,{}_c a^k_{11}\,{}_d a^k_{11}\mathcal{K}^k_X - {}_c a^k_{12}\,{}_d a^k_{12}\mathcal{K}^k_Y - {}_c a^k_{13}\,{}_d a^k_{13}\mathcal{K}^k_Z\right)\,{}^x_c F^k_{\alpha_{u_x}}\,{}^x_d F^k_{\beta_{u_x}} \\ K^{k\,\alpha\,{}_d u_x\,\beta\,{}_d u_x\,ll}_{{}_d u_x\,{}_d u_x} &= \left({}_d a^k_{11}\,{}_d a^k_{11}\mathcal{K}^k_X + {}_d a^k_{12}\,{}_d a^k_{12}\mathcal{K}^k_Y + {}_d a^k_{13}\,{}_d a^k_{13}\mathcal{K}^k_Z\right)\,{}^x_d F^k_{\alpha_{u_x}}\,{}^x_d F^k_{\beta_{u_x}} \end{aligned}$$

More details, omitted here for brevity, are reported in Appendix C of ref. [34].

This formulation has the drawback that the springs impose the compatibility of the displacements only for a single point along the thickness of layer k. To have the compatibility enforced in a *weak form* in the thickness direction, one may use a *distribution* of springs. This is now discussed.

Let the stiffnesses *per unit of length of thickness* of element c (or d, being the thickness of each layer the same according to the assumption earlier introduced) of the springs be indicated with $\mathcal{S}^k_X$, $\mathcal{S}^k_Y$, and $\mathcal{S}^k_Z$ (they are assumed constant and not a function of the layer's thickness coordinate). Let h_k be the layer thickness (the same for both elements). The potential energy is the following:

$$\mathcal{U}_k = \frac{1}{2} \int_{h_k} \left[\begin{bmatrix} {}_c u^k_{Xj} \\ {}_c u^k_{Yj} \\ {}_c u^k_{Zj} \end{bmatrix} - \begin{bmatrix} {}_d u^k_{Xl} \\ {}_d u^k_{Yl} \\ {}_d u^k_{Zl} \end{bmatrix} \right]^T \begin{bmatrix} \mathcal{S}^k_X & 0 & 0 \\ 0 & \mathcal{S}^k_Y & 0 \\ 0 & 0 & \mathcal{S}^k_Z \end{bmatrix} \left[\begin{bmatrix} {}_c u^k_{Xj} \\ {}_c u^k_{Yj} \\ {}_c u^k_{Zj} \end{bmatrix} - \begin{bmatrix} {}_d u^k_{Xl} \\ {}_d u^k_{Yl} \\ {}_d u^k_{Zl} \end{bmatrix} \right] \mathrm{d}z \tag{34}$$

(observe that it always is $\mathrm{d}z = \mathrm{d}z^k$).

Equation 34 can be written in a very similar to equation 33 form. However, the stiffness terms are now different. For example, it is

$$K^{k\,\alpha_{\,cu_z}\beta_{\,du_z}jl}_{\,cu_z\,du_z} = \left(-\,{}_c a^k_{31}\,{}_d a^k_{31}\mathcal{S}^k_X - \,{}_c a^k_{32}\,{}_d a^k_{32}\mathcal{S}^k_Y - \,{}_c a^k_{33}\,{}_d a^k_{33}\mathcal{S}^k_Z\right) \int_{z_{\mathrm{bot}_k}}^{z_{\mathrm{top}_k}} {}^z_c F^k_{\alpha_{u_z}}\left(z^k\right)\, {}^z_d F^k_{\beta_{u_z}}\left(z^k\right) \mathrm{d}z \tag{35}$$

The formulation reported in equation 34 corresponds to the actual implementation of the present GUF-based capability. Note that the integral of equation 35 can be solved numerically. The theoretical derivations used to enforce the interelement compatibility and the boundary condition (connection of the structure to the ground) are explained next with particular focus on the thickness assembling of the matrices.

7.3 Thickness Assembling of the Springs' Contributions

First the assembling of the finite element stiffness matrices is discussed. Then how the springs modify the resulting matrix is present.

7.3.1 Thickness Assembling of the Finite Element Stiffness Matrix

For simplicity of the discussion assume that both elements c and d have 3 nodes only and are made of two layers.

Suppose that for element c the adopted theory is ${}_{EZL}PVD_{211}$ (see ref. [34] for the more details on the acronym):

$$\begin{cases} u_x = u_{x0} + z\phi_{1_{u_x}} + z^2\phi_{2_{u_x}} \\ u_y = u_{y0} + z\phi_{1_{u_y}} + (-1)^k \zeta_k u_{yZ} \\ u_z^k = \dfrac{P_0^k + P_1^k}{2} u_{z_t}^k + \dfrac{P_0^k - P_1^k}{2} u_{z_b}^k \end{cases} \tag{36}$$

Thus, it is clear that the number of terms (DOFs in the thickness direction) is the following: ${}_c\mathcal{N}_{u_x} = 3$, ${}_c\mathcal{N}_{u_y} = 3$, and ${}_c\mathcal{N}_{u_z} = 2$. P_0^k and P_1^k are the constant and linear Legendre polynomials.

Suppose that for element d a different theory is adopted. For example assume that ${}_{LZL}PVD_{111}$ (see ref. [34] for the more details on the acronym) is used:

$$\begin{cases} u_x^k = \dfrac{P_0^k + P_1^k}{2} u_{x_t}^k + \dfrac{P_0^k - P_1^k}{2} u_{x_b}^k \\ u_y = u_{y0} + z\phi_{1_{u_y}} + (-1)^k \zeta_k u_{yZ} \\ u_z^k = \dfrac{P_0^k + P_1^k}{2} u_{z_t}^k + \dfrac{P_0^k - P_1^k}{2} u_{z_b}^k \end{cases} \tag{37}$$

Thus, it is clear that ${}_d\mathcal{N}_{u_x} = 2$, ${}_d\mathcal{N}_{u_y} = 3$, and ${}_d\mathcal{N}_{u_z} = 2$.

It should be emphasized that within GUF formalism the ESL theories do not have index k (except for the Zig-Zag term). However, when the matrix at layer level is derived the index k is considered for consistency of the notation. The assembling in the thickness direction will take care of the ESL or LW description for the different quantities.

Focus is now on the assembling of matrix $\mathbf{K}^k_{u_x u_y}$. Figure 12 shows one of the terms of the matrix at layer and nodal levels. The subscript c is added for clarity. Figure 13 shows the matrix at layer and element levels, whereas Figure 14 presents the matrix after the assembling in the thickness direction is completed. It should be observed that both displacements u_x and u_y of element c have an ESL description. Thus, all the terms of the stiffness matrix need to be added as shown in Figure 14. Things would be different if one variable (or both) had a LW description. In that case only some elements would be added in correspondence of the degrees of freedom at the interface between layers and Figure 14 would be modified.

The other finite element matrices are built with similar logic (details are omitted for brevity).

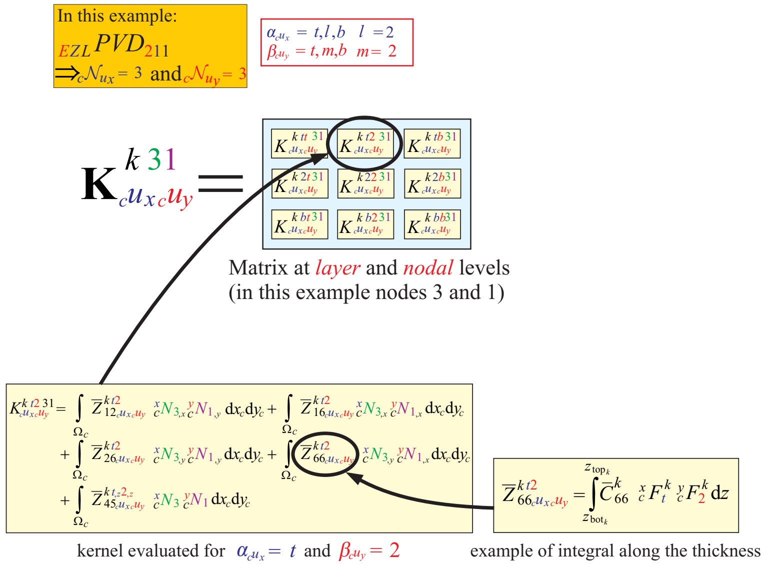

Fig. 12. Finite element implementation of the Generalized Unified Formulation: expansion of the thickness indices to obtain the stiffness matrix at layer, and nodal levels. Example for matrix $\mathbf{K}^{k\,31}_{c u_x\, c u_y}$.

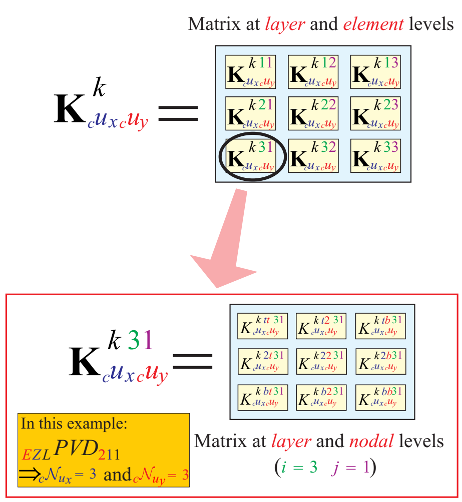

Fig. 13. Finite element implementation of the Generalized Unified Formulation: expansion of the finite element indices i and j to obtain the matrix at layer and element levels. Example for matrix $\mathbf{K}^{k}_{c u_x\, c u_y}$ (see also Figure 12).

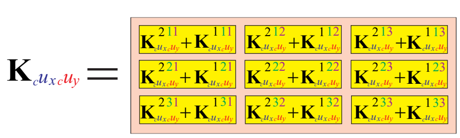

Fig. 14. Finite Element implementation of the Generalized Unified Formulation: example of element matrix $\mathbf{K}_{c u_x\, c u_y}$.

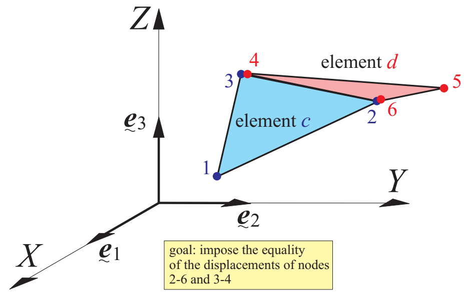

Fig. 15. Two triangles c and d.

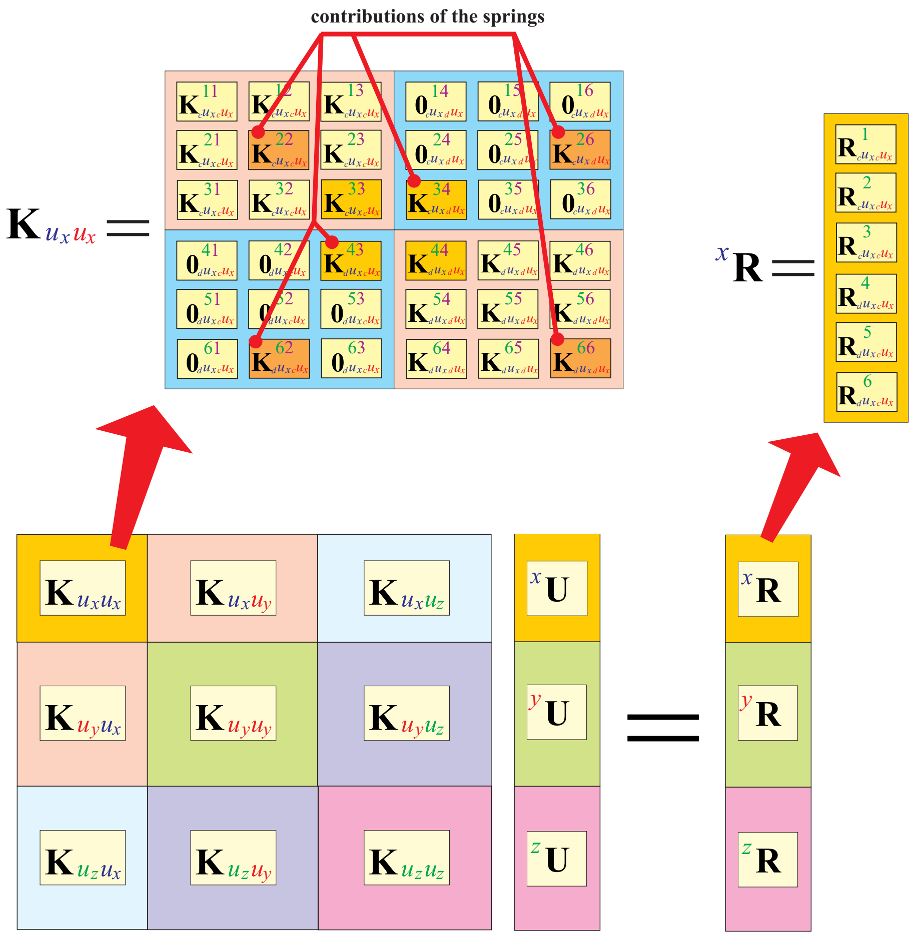

Fig. 16. Two triangles c and d. Final system of equations that needs to be solved

7.3.2 Spring Contributions

Assume that the two elements are located in space as in Figure 15. The goal is to impose the compatibility between the displacements of node 3 and node 4 and between 2 and 6. Suppose for simplicity that the structure is made of two layers, and that the values of $\mathcal{S}_X^k, \mathcal{S}_Y^k, \mathcal{S}_Z^k$ are assigned and known (in this implementation all the spring stiffness densities are taken to be 10^3 times the highest entry of the stiffness matrix, numerically obtained). The final set of equations that needs to be solved is depicted in Figure 16. This formulation

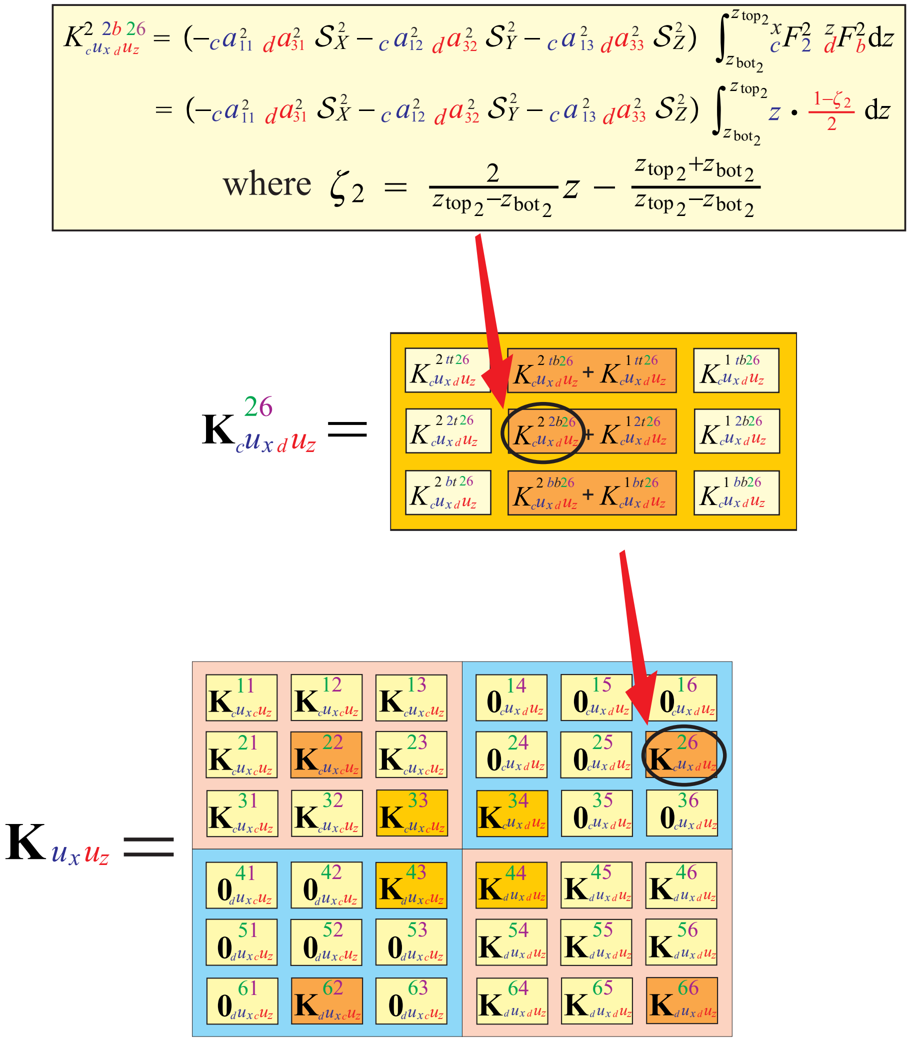

Fig. 17. Imposition of the compatibility of displacements. Case of matrix $\mathbf{K}^{26}_{cu_x\,du_z}$.

has the following properties:

- All the different entries of the displacement vector have to be understood in local coordinate systems of the respective finite elements and not in the global coordinate system.
- The loads are also provided in local element coordinate systems.
- The conceptual structure made of two elements and shown in the example of Figure 15, needs to be constrained to the ground. This will be discussed later.

Figures 17 and 18 show how the boundary conditions via springs are imposed. The reader should focus the attention on the thickness integrals.

The particular assembling in the thickness direction implies that at the nodes where the springs are used there is the *interlaminar compatibility of displacements* referred to *different coordinate systems* (in fact, the two elements have

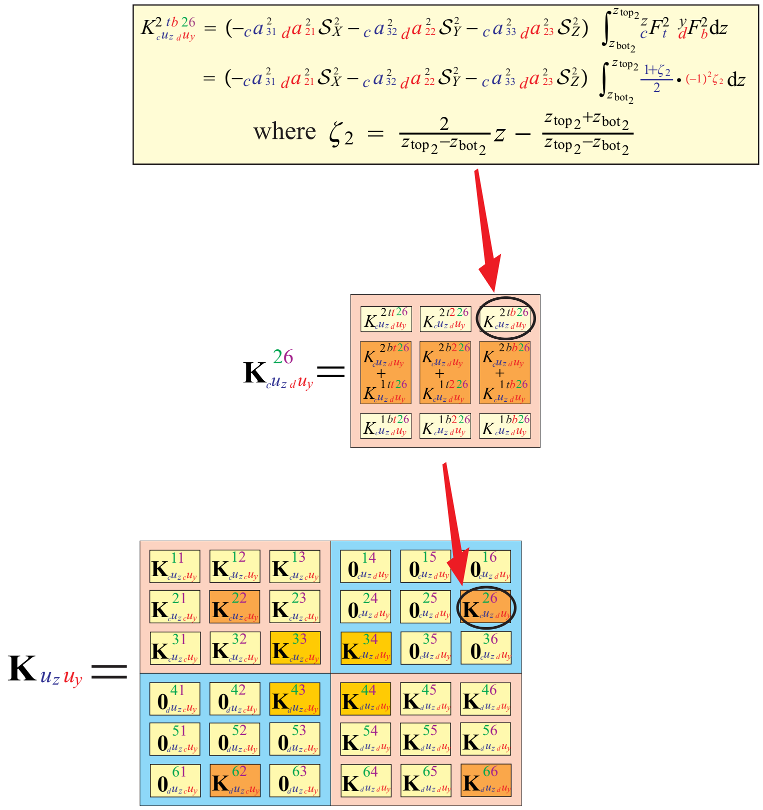

Fig. 18. Imposition of the compatibility of displacements. Case of matrix $\mathbf{K}^{26}_{c u_z\, d u_y}$.

different coordinate systems). This is the case, for example, when matrix $\mathbf{K}^{26}_{c u_z\, d u_y}$ is built.

The structure has to be restrained to the ground. How this is obtained in this formulation is now discussed. Suppose that node 1 of element c is grounded (i.e., the displacements of node 1 have to be imposed to be zero). This is achieved as shown in Figure 19. As previously discussed, it is also possible to ground only a specific point (or a finite number of points) in the thickness direction (for a given finite element node). The procedure is identical to the one described in Figure 19. However, there is no thickness integral (as in the weak imposition of the compatibility condition) and only the contribution of the layer specifically involved by the spring connection is a non-zero quantity.

Note that in the interpretation of Figures 18 and 19, the superscript "2" indicating the identity of layer 2 should not be confused with the exponent 2.

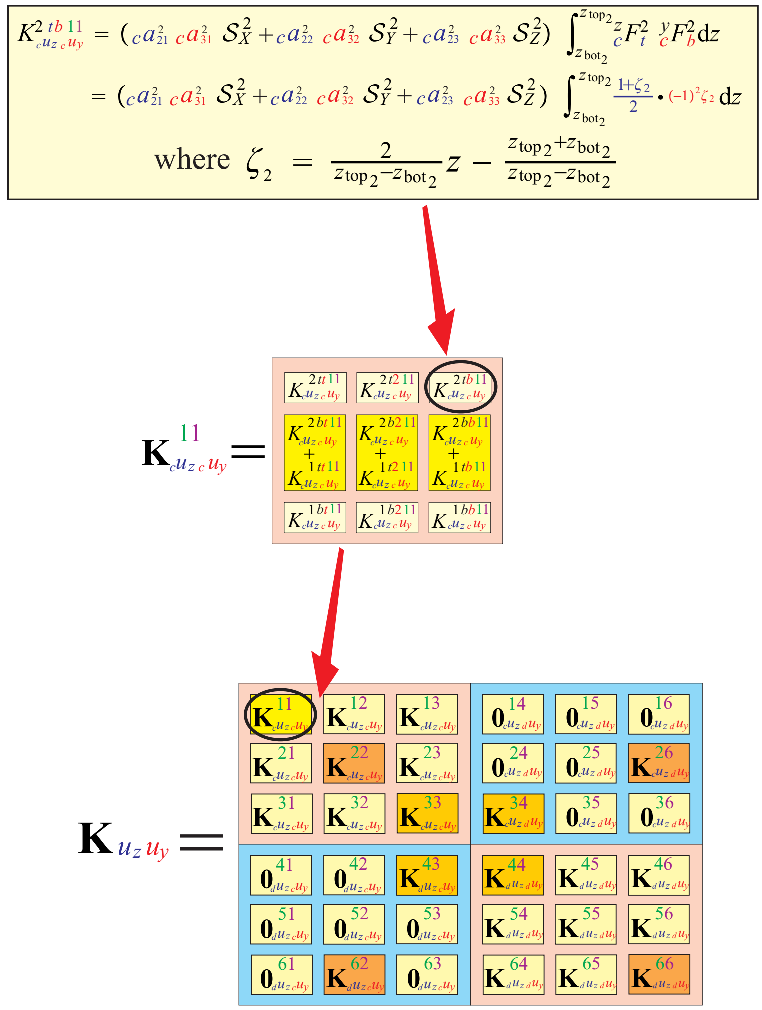

Fig. 19. Imposition of the ground conditions for node 1 of element c. Details relative to matrix $\mathbf{K}^{11}_{c u_z\, d u_y}$.

8 Implemented Triangular Elements

GUF is a very general technique: it can be applied to different types of axiomatic approaches such as the global-local model [70, 71] or different finite element formulations (see refs. [49, 47]). In the present work GUF finite element implementation includes linear, parabolic, cubic, and quartic triangular elements (see Figure 20). The results of the present work have all been obtained with quartic triangular element, which for the investigated cases showed excellent numerical performances. All the details regarding the finite element implementation are reported in the extended conference version of this work (ref. [34]).

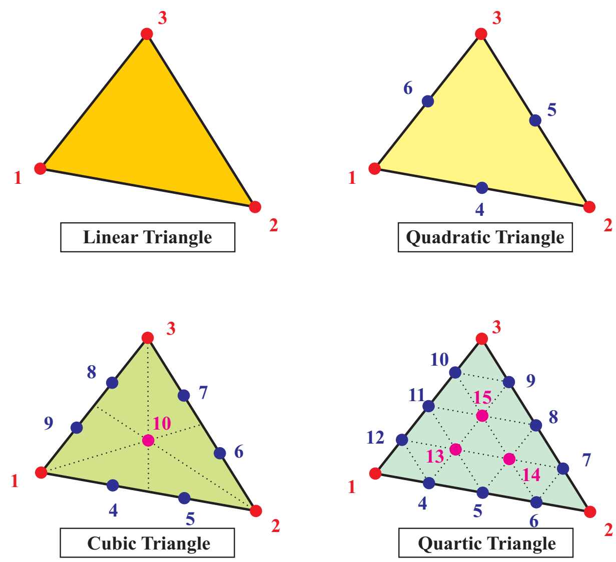

Fig. 20. Linear and higher order triangles: local node numbering.

9 Results

The global coordinate system X, Y, Z is located at the center of the plate (see Figure 21). The edges have length a and b (in the X and Y directions respectively). They are selected to be the same. In this work the loading condition is represented by a transverse constant distributed load. Two-layer and three-layer structures are examined. In the material coordinate system (which is variable in the space being the fibers' patterns curvilinear) the properties are assumed orthotropic and reported in Figure 21.

Called T_0^k and T_1^k the angles the fibers form with respect to the X axis at $X = 0$ (center) and $X = a/2$ (edge) respectively, the fibers' angle is selected to change with the in-plane coordinates as follows:

$$\vartheta^k(X) = \frac{2\left(T_1^k - T_0^k\right)}{a}|X| + T_0^k \tag{38}$$

Several cases are analyzed and combined in this work. They are described in Figs. 22 and 23 where the fibers' patterns are shown and the corresponding values for the parameters T_0 and T_1 (see equation 38) provided. Note that in Figs. 22 and 23 the superscript k, indicating the layer ID, is not used because the cases presented can be adopted to any layer in the investigations carried out in this work.

Table 1 presents the normalized central displacement for a two-layer structure loaded with a constant distributed load equal to 10 kN/m^2 (see ref. [76]). The first layer has thickness $h/2$ and angles T_0^1 and T_1^1 corresponding to case 4 (see Figure 22). The second layer has variable parameters used to describe

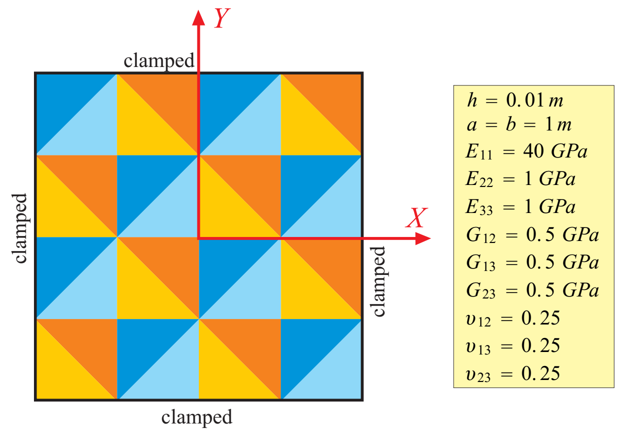

Fig. 21. Geometry, material properties of the layers, and mesh used for this test case (quartic triangular elements).

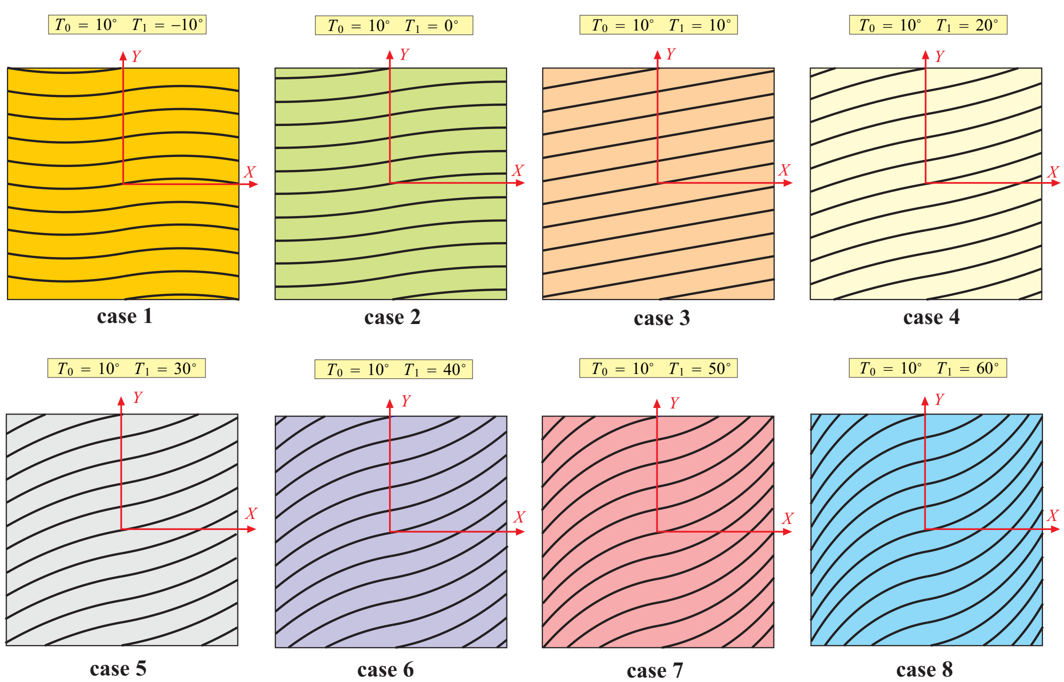

Fig. 22. Different patterns for the curvilinear fibers.

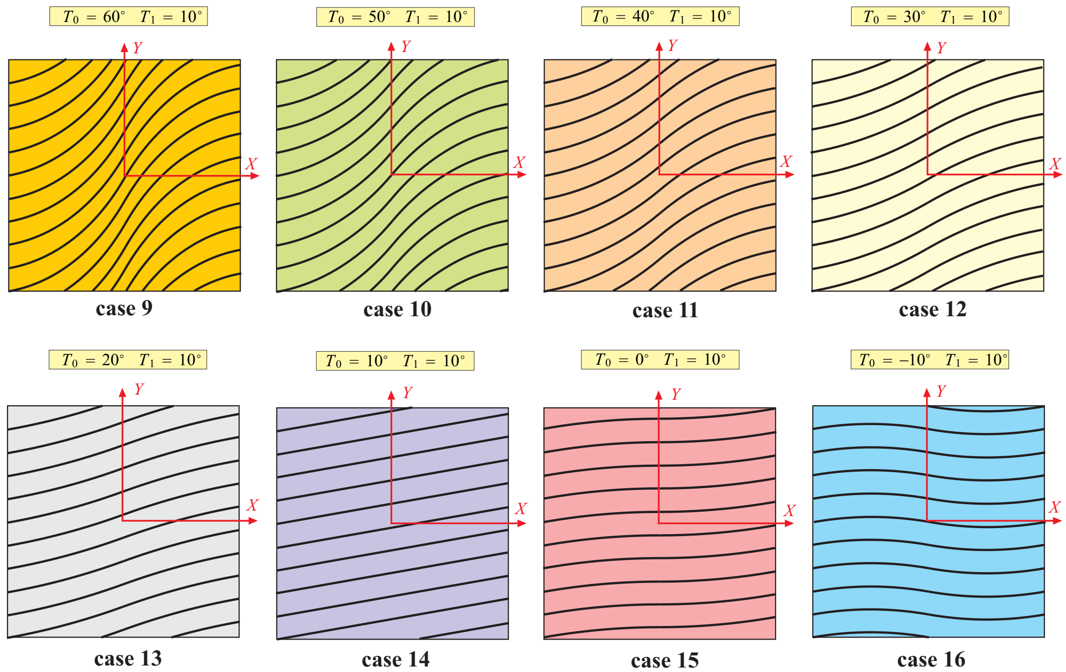

Fig. 23. Different patterns for the curvilinear fibers.

the curvilinear fibers (cases $1-8$ of Figure 22). In Table 2 the first layer has

Layer 1			Layer 2			u_z/h	
T_0^1	T_1^1	Case	T_0^2	T_1^2	Case	Present	Ref [76]
10°	20°	4	10°	−10°	1	1.409	(1.405)
10°	20°	4	10°	0°	2	1.210	(1.204)
10°	20°	4	10°	10°	3	1.032	(1.019)
10°	20°	4	10°	20°	4	0.993	(0.978)
10°	20°	4	10°	30°	5	1.131	(1.125)
10°	20°	4	10°	40°	6	1.353	(1.360)
10°	20°	4	10°	50°	7	1.577	(1.589)
10°	20°	4	10°	60°	8	1.766	(1.773)

Table 1
Normalized central deflection u_z/h of a two-layer unsymmetric clamped Variable Stiffness Composite Laminate under a transverse distributed load equal to $10\ kN/m^2$. The present results have been obtained using the $_{LLL}PVD_{111}$ theory.

thickness $h/2$ and angles T_0^1 and T_1^1 corresponding to case 13 (see Figure 23). The second layer has variable parameters used to describe the curvilinear fibers (cases 9 div 16 of Figure 23). Table 3 presents the normalized central displacement for a three-layer structure (see ref. [76]). All layers have thickness equal to $h/3$. In the first layer the angles T_0^1 and T_1^1 correspond to case 4 (see Figure 22). The second layer has angle parameters corresponding to case 5

Layer 1			Layer 2			u_z/h	
T_0^1	T_1^1	Case	T_0^2	T_1^2	Case	Present	Ref [76]
20°	10°	13	−10°	10°	16	1.234	(1.210)
20°	10°	13	0°	10°	15	1.106	(1.084)
20°	10°	13	10°	10°	14	0.992	(0.973)
20°	10°	13	20°	10°	13	0.972	(0.956)
20°	10°	13	30°	10°	12	1.065	(1.048)
20°	10°	13	40°	10°	11	1.207	(1.187)
20°	10°	13	50°	10°	10	1.340	(1.319)
20°	10°	13	60°	10°	9	1.445	(1.425)

Table 2
Normalized central deflection u_z/h of a two-layer unsymmetric clamped Variable Stiffness Composite Laminate under a transverse distributed load equal to 10 kN/m^2. The present results have been obtained using the $_{LLL}PVD_{111}$ theory.

Layer 1			Layer 2			Layer 3			u_z/h	
T_0^1	T_1^1	Case	T_0^2	T_1^2	Case	T_0^3	T_1^3	Case	Present	Ref [76]
10°	20°	4	10°	30°	5	10°	−10°	1	2.469	(2.425)
10°	20°	4	10°	30°	5	10°	0°	2	2.213	(2.177)
10°	20°	4	10°	30°	5	10°	10°	3	2.014	(1.983)
10°	20°	4	10°	30°	5	10°	20°	4	1.998	(1.971)
10°	20°	4	10°	30°	5	10°	30°	5	2.257	(2.232)
10°	20°	4	10°	30°	5	10°	40°	6	2.694	(2.670)
10°	20°	4	10°	30°	5	10°	50°	7	3.105	(3.071)
10°	20°	4	10°	30°	5	10°	60°	8	3.386	(3.331)

Table 3
Normalized central deflection u_z/h of a three-layer unsymmetric clamped Variable Stiffness Composite Laminate under a transverse distributed load equal to 20 kN/m^2. The present results have been obtained using the $_{LLL}PVD_{111}$ theory.

This is the accepted manuscript of the paper published on Composite Structures. DOI: https://doi.org/10.1016/j.compstruct.2015.05.022 34

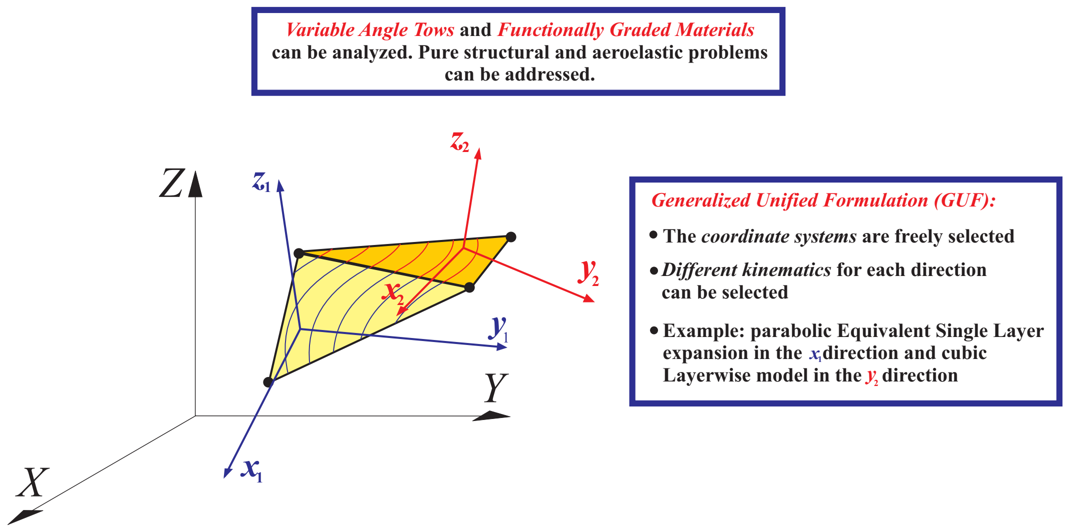

Fig. 24. Main properties of the Generalized Unified Formulation for Variable Stiffness Composite Laminates.

(see Figure 22). The third layer presents variable angle parameters used to describe the curvilinear fibers (cases $1-8$ of Figure 22).

There is an excellent correlation with published data. With the generality of the GUF-based approach several studies regarding the displacements and stresses distributions will be analyzed by changing theories and orders of expansions in the different directions. Being the fibers curvilinear, it is anticipated that for Variable Stiffness Composite Laminates GUF will provide a useful investigation tool since each direction is independently handled and this can be freely changed by the user.

Finally, the above discussed extension of the Generalize Unified Formulation framework to analyze Variable Angle Tows (or Variable Stiffness Composite Laminate) is summarized in Figure 24.

10 Conclusions

This work presented for the first time the Generalized Unified Formulation extended to the case of *Variable Angle Tow* composite structures. Functionally graded properties in both the thickness and in-plane direction have also been theoretically formulated. The numerical implementation was based on a quartic triangular shell element with user-defined curvilinear fiber directions. Main features of the proposed computational framework for *Variable Stiffness Composite Laminates* are the following:

- An Equivalent Single Layer or Layer Wise description for a displacement in *any* element-wise direction can be selected. This feature allows the user to concentrate the computational effort where it is necessary (case dependent property). Optimization and reliability analysis are then natural applications.
- The thickness axiomatic expansion of a displacement along a generic direction is completely independent of the choice made for another direction. For example, a cubic Higher Order Theory can be used for a local in-plane displacement and a linear Layer Wise approach can be adopted for a local transverse displacement variable.
- Equivalent Single Layer expansions can be enhanced with Murakami's Zig Zag functions.
- Spatially variable thickness and material properties are included in the formulation.
- Several different finite elements can be adopted with no additional programming effort thanks to the theory-invariant kernels of the Generalized Unified Formulation from which an infinite number of theories can be generated.
- The interelement displacement compatibility is imposed with the penalty method (weak form). This has proven to be efficient and provides to the user great versatility since the finite elements are independently modeled (different theories for user-selected directions).
- The interlaminar displacement compatibility is automatically enforced via thickness assembling of the finite element matrices.
- No shear correction factors are required and the transverse strain effects can be retained.

The results showed excellent correlation with available data on Variable Stiffness Composite Laminates regarding two- and three-layer unsymmetric multilayer structures.

Future works will assess the performance of a large number of theories which will exploit the generality of the Generalized Unified Formulation. Moreover, mixed variational approaches will also be investigated for an a-priori interlaminar transverse stress equilibrium enforcement.

11 Acknowledgment

This paper is dedicated to the memory of *Todd O. Williams* (Los Alamos National Lab, Theoretical Division) for his contributions to the theoretical modeling of structures.

References

[1] V. Aitharaju and R. Averill. C^0 Zig-Zag Finite Element for Analysis of Laminated Composite Beams. *J Eng Mech ASCE*, 125:323–330, 1999.

[2] Hamed Akhavan, Pedro Ribeiro, and Marcelo F. S. F. de Moura. Damage onset on tow-placed variable stiffness composite laminates. *Composite Structures*, 113:419–428, 2014.

[3] Hamed Akhavan, Pedro Ribeiro, and M.F.S.F de Moura. Large deflection and stresses in variable stiffness composite laminates with curvilinear fibres. *Composite Structures*, 73:14–26, 2013.

[4] M. M. Alipour and M. Shariyat. An Elasticity-Equilibrium-Based Zig-Zag Theory for Axisymmetric Bending and Stress Analysis of the Functionally Graded Circular Sandwich Plates, Using a Maclaurin-Type Series Solution. *European Journal of Mechanics A/Solids*, 34:78–101, 2012.

[5] R. Averill and Y. Yip. Thick Beam Theory and Finite Element Model with Zig-Zag Sublaminate Approximations. *AIAA Journal*, 34:1627–1632, 1996.

[6] R. C. Batra and S. Vidoli. Higher order piezoelectric plate theory derived from a three-dimensional variational principle. *AIAA Journal*, 40:91–104, 2002.

[7] H. Ben Dhia. Numerical modelling of multiscale problems: the arlequin method. 1995. In: CD Proceedings ECCM'99, Munchen; 1999.

[8] H. Ben Dhia. Multiscale mechanical problems: the arlequin method. *Comptes Rendus de l'academie des Sciences Series IIB Mechanics Physics Astronomy*, 326:899–904, 1998.

[9] H. Ben Dhia and G. Rateau. The arlequin method as a flexible engineering tool. *International Jounral for Numerical Methods in Engineering*, 62:1442–1462, 2005.

[10] F. Biscani, G. Giunta, S. Belouettar, E. Carrera, and H. Hu. Variable kinematic beam elements coupled via arlequin method. *Composite Structures*, 93:697–708, 2011.

[11] S. Brischetto, E. Carrera, and L. Demasi. Free vibration of sandwich plates and shells by using Zig-Zag function. *Shock and Vibration*, 2010. in press.

[12] S. Brischetto, E. Carrera, and L. Demasi. Improved bending analysis of sandwich plates using Zig-Zag functions. *Composite Structures*, 2010. in press.

[13] S. Brischetto, E. Carrera, and L. Demasi. Improved response of unsymmetrically laminated sandwich plates by using Zig-Zag functions. *Journal of Sandwich Structures & Materials*, 2010. in press.

[14] E. Carrera. A class of two-dimensional theories for anisotropic multilayered plates analysis. *Accademia delle Scienze Torino*, pages 19–20,1–39, 1995-1996.

[15] E. Carrera. Evaluation of Layer-Wise Mixed Theories for Laminated Plates Analysis. *American Institute of Aeronautics and Astronautics*

Journal, 26:830–839, 1998.

[16] E. Carrera. Mixed Layer-Wise Models for Multilayered Plates Analysis. *Composite Structures*, 43:57–70, 1998.

[17] E. Carrera. Historical review of Zig-Zag theories for multilayered plates and shells. *App Mech Rev*, 56, 2003.

[18] E. Carrera. Theories and Finite Elements for Multilayered Plates and Shells: A Unified Compact Formulation with Numerical Assessment and Benchmarking. *Archives of Computational Methods in Engineering*, 10:215–296, 2003.

[19] E. Carrera. On the Use of Murakami's Zig-Zag Function in the Modeling of Layered Plates and Shells. *Composite Structures*, 82:541–554, 2004.

[20] K. N. Cho, C. W. Bert, and A. G. Striz. Free Vibrations of Laminated Rectangular Plates Analyzed by Higher Order Individual-Layer Theory. *Journal of Sound and Vibration*, 145:429–442, 1991.

[21] Byung Chul Kim, Paul M. Weaver, and Kevin Potter. Manufacturing characteristics of the continuous tow shearing method for manufacturing of variable angle tow composites. *Composite: Part A*, 61:141–151, 2014.

[22] B.H. Coburn, Z. Wu, and P.M. Weaver. Buckling analysis of stiffened variable angle tow panels. *Composite Structures*, 111:259–270, 2014.

[23] T.D. Dang and S.R. Hallett. A numerical study on impact and compression after impact behavior of variable angle tow laminates. *Composite Structures*, 96:194–206, 2013.

[24] L. Demasi. Refined multilayered plate elements based on Murakami Zig-Zag functions. *Composite Structures*, 70:308–16, 2005.

[25] L. Demasi. 2D, quasi 3D and 3D Exact Solutions for Bending of Thick and Thin Sandwich Plates. *Journal of Sandwich Structures & Materials*, 10:271–310, 2008.

[26] L. Demasi. ∞^3 hierarchy plate theories for thick and thin composite plates. *Composite Structures*, 84:256–270, 2008.

[27] L. Demasi. ∞^6 mixed plate theories based on the generalized unified formulation. Part I: Governing Equations. *Composite Structures*, 87:1–11, 2009.

[28] L. Demasi. ∞^6 mixed plate theories based on the Generalized Unified Formulation. Part II: Layerwise Theories. *Composite Structures*, 87:12–22, 2009.

[29] L. Demasi. ∞^6 mixed plate theories based on the Generalized Unified formulation. Part III: Advanced Mixed High Order Shear Deformation Theories. *Composite Structures*, 87:183–194, 2009.

[30] L. Demasi. ∞^6 mixed plate theories based on the Generalized Unified Formulation. Part IV: Zig-Zag Theories. *Composite Structures*, 87:195–205, 2009.

[31] L. Demasi. ∞^6 mixed plate theories based on the Generalized Unified Formulation. Part V: Results. *Composite Structures*, 88:1–16, 2009.

[32] L. Demasi. Invariant Finite Element Model for Composite Structures: the Generalized Unified Formulation. *AIAA Journal*, 48:1602–1619, 2010.

[33] L. Demasi. Partially layer wise advanced zig-zag and hsdt models based on the generalized unified formulation. *Engineering Structures*, 53:63–91, 2013.

[34] L. Demasi, Y. Ashenafi, R. Cavallaro, and E. Santarpia. Generalized unified formulation shell element for functionally graded variable-stiffness composite laminates and aeroelastic applications. Number AIAA 2015-0195. 56th AIAA/ASME/ASCE/AHS/ASC Structures, Structural Dynamics, and Materials Conference, Missimmee, Florida, American Institute of Aeronautics and Astronautics, 5-9 January 2015.

[35] L. Demasi and E. Livne. Structural ritz-based simple-polynomial nonlinear equivalent plate approach: An assessment. *Journal of Aircraft*, 43:1685–1697, 2006.

[36] C.A. Felippa. Error analysis of penalty function techniques for constraint definition in linear algebraic system. *International Journal for Numerical Methods in Engineering*, 11:709–728, 1977.

[37] R.M.J. Groh and P.M. Weaver. Buckling analysis of variable angle tow, variable thickness panels with transverse shear effects. *Composite Structures*, 107:482–493, 2014.

[38] M.W. Hyer and H.H. Lee. The use of curvilinear fiber format to improve buckling resistance of composite plates with central circular holes. *Composite Structures*, 18:239–261, 1991.

[39] T. Kant and K. Swaminathan. Free vibration of isotropic, orthotropic, and multilayer plates based on higher order refined theories. *Journal of Sound and Vibration*, 241:319–327, 2001.

[40] S. Kapuria, P. Dumir, and A. Ahmed. An Efficient Higher Order Zig-Zag Theory for Composite and Sandwich Beams Subjected to Thermal Loading. *Int J Solids Struct*, 40:6613–6631, 2003.

[41] B. C. Kim, K. Potter, and P.M. Weaver. Continuous tow shearing for manufacturing variable angle tow composites. *Composite Structures*, 43:1347–1356, 2012.

[42] G. Kirchhoff. *Über* das Gleichgewicht und diw Bewegung einer elasticien scheibe. *Journal für die reine und angewandte Mathematik*, 40:51–88, 1850.

[43] CS Lopes, PP Camanho, Z Gürdal, and BF Tatting. Progressive failure analysis of tow-placed variable-stiffness composite panels. *Int J Solids Struct*, 44:8493–8516, 2007.

[44] J. L. Mantari, A. S. Oktem, and C. G. Soares. Static and Dynamic Analysis of Laminated Composite and Sandwich Plates and Shells by Using a new Higher-Order Shear Deformation Theory. *Composites Structures*, 94:37–49, 2011.

[45] J. L. Mantari, A. S. Oktem, and C. G. Soares. A new Trigonometric Shear Deformation Theory for Isotropic, Laminated Composite and Sandwich Plates. *International Journal of Solids and Structures*, 49:43–53, 2012.

[46] Mindlin. Influence of rotatory inertia and shear in flexural motion of isotropic elastic plates. *Journal of Applied Mechanics*, 18:1031–1036,

1951.

[47] S. Morganti, F. Auricchio, D. J. Benson, F.I. Gambarin, S. Hartmann, T.J.R. Hughes, and A. Reali. Patient-specifi isogeometric structural analysis of aortic valve. *Computer Methods in Applied Mechanics and Engineering*, 284:508–520, 2015.

[48] H. Murakami. Laminated composite plate theory with improved in-plane response. *Journal of Applied Mechanics*, 53:661–666, 1986.

[49] A. P. Nagy and D. J. Benson. On the numerical integration of trimmed isogeometric elements. *Computer Methods in Applied Mechanics and Engineering*, 284:165–185, 2015.

[50] A. Nosier, R. K. Kapania, and J. N. Reddy. Free Vibration Analysis of Laminated Plates Using a Layer-Wise Theory. *AIAA Journal*, 31:2335–2346, 1993.

[51] P. F. Pai and A. N. Palazotto. A Higher-Order Sandwich Plate Theory Accounting for 3D Stresses. *International Journal of Solids and Structures*, 38:5045–5062, 2001.

[52] B. N. Pandit, B. N. Singh, and A. H. Sheikh. Buckling Response of Sandwich Plate with Random Material Properties Using an Improved Higher Order Zig-Zag Theory. *AIAA Journal*, 47:418–428, 2009.

[53] A. S. Panesar, K. Hazra, and P.M. Weaver. Investigation of thermally induced bistable behaviour for tow-steered laminates. *Composites: Part A*, 43:926–934, 2012.

[54] L. F. Qian, R. C. Batra, and L. M. Chen. Static and dynamic deformations of thick functionally graded elastic plates by using higher-order shear and normal deformable plate theory and meshless local Petrov-Galerkin method. *Compos Part B: Eng*, 35:685–97, 2004.

[55] D. T. Raju and S. Kumar. Transient Analysis of Composite Laminated Plates Using Higher-Order Shear Deformation Theory with Zig-Zag Function. *International Journal of Applied Engineering Research, Dindigul*, 2:562–569, 2011.

[56] G. Raju, Z. Wu, B. C. Kim, and P.M. Weaver. Prebuckling and buckling analysis of variable angle tow plates with general boundary conditions. *Composite Structures*, 94:2961–2970, 2012.

[57] G. Raju, Z. Wu, and P.M. Weaver. Postbuckling analysis of variable angle tow plates using differentia quadrature method. *Composite Structures*, 106:74–84, 2013.

[58] J. N. Reddy. An evaluation of equivalent single layer and layerwise theories of composite laminates. *Composite Structures*, 25:21–35, 1993.

[59] J. N. Reddy. Mechanics of Laminated Composite Plates, Theory and Analysis. 2004. (2nd edn), CRC Press.: Boca Raton, London, New York, Washington, D. C.

[60] E. Reissner. The effect of transverse shear deformation on the bending of elastic plates. *Journal of Applied Mechanics*, 12:69–76, 1945.

[61] D. H. Robbins and J. N. Reddy. Modelling of thick composites using a layerwise laminate theory. *International Journal for Numerical Methods*

in Engineering, 36:655–677, 2005.

[62] J. D. Rofrigues, C. M. C. Roque, A. J. M. Ferreira, E. Carrera, and M. Cinefra. Radial Basis Functions-Finite Differences Collocation and a Unified Formulation for Bending, Vibration and Buckling Analysis of Laminated Plates, According to Murakami's Zig-Zag Theory. *Composite Structures*, 93:1613–1620, 2011.

[63] A. Sabik and I. Kreja. Linear Analysis of Laminated Multilayered Plates with the Application of Zig-Zag Function. *Archives of Civil and Mechanical Engineering*, 8:61–72, 2008.

[64] O. Stodieck, J.E. Cooper, P.M. Weaver, and P. Kealy. Improved aeroelastic tailoring using tow-steered composites. *Composite Structures*, 106:703–715, 2013.

[65] K. Swaminathan and S. S. Patil. Analytical solutions using higher order refined computational model with 12 degrees of freedom for the free vibration analysis of antisymmetric angle-ply plates. *Composite Structures*, 2007. doi: 10.1016/j.compstruct.2007.01.001.

[66] P. Vidal and O. Polit. A Sine Finite Element Using a Zig Zag Function for the Analysis of Laminated Composite Beams. *Composites: Part B*, 42:1671–1682, 2011.

[67] T. A. Weisshaar and D. H. Lee. Aeroelastic tailoring of joined-wing configurations. 43nd AIAA/ASME/ASCE/AHS/ASC Structures, Structural Dynamics and Materials Conference, Denver, CO, 22-25 April 2002.

[68] S.C. White, G. Raju, and P. M. Weaver. Initial post-buckling of variable-stiffness curved panels. *Journal of the Mechanics and Physics of Solids*, 71:132–155, 2014.

[69] T. O. Williams. A generalized, multilength scale framework for thermo-diffusionally-mechanically coupled, nonlinear, laminated plate theories with delaminations. *International Journal of Solids and Structures*, 42:1465–1490, 2005.

[70] T. O. Williams. A New Theoretical Framework for the Formulation of General, Nonlinear, Multiscale Plate Theories. *International Journal of Solids and Structures*, 45:2534–2560, 2008.

[71] T. O. Williams. A new, unified, theoretical framework for the formulation of general nonlinear, single-scale shell theories. *Composite Structures*, 107:544–558, 2014.

[72] K. C. wu, B. K. Stanford, G.A. Hrinda, Z. Wang, R.A. Martin, and H.A. Kim. Structural assessment of advanced composite tow-steered shells. Number AIAA 2013-1769. 54rd AIAA/ASME/ASCE/AHS/ASC Structures, Structural Dynamics, and Materials Conference, Boston, Massachusetts, American Institute of Aeronautics and Astronautics, 8-11 April 2013.

[73] Z. Wu, G. Raju, and P.M. Weaver. Postbuckling analysis of variable angle tow composite plates. *International Journal of Solids and Structures*, 50:1770–1780, 2013.

[74] Z. Wu, P.M. Weaver, and G. Raju. Postbuckling optimization of variable

angle tow composite plates. *Composite Structures*, 103:34–42, 2013.

[75] Y. K. Wu Zhen, SH Lo Cheung, and W. Chen. Effects of Higher-Order Global-Local Shear Deformations on Bending, Vibration and Buckling of Multilayered Plates. *Composite Structures*, 2007. DOI: 10.1016/j.compstruct.2007.01.017.

[76] Saleh Yazdani and Pedro Ribeiro. Geometrically non-linear static analysis of unsymmetric composite plates with curvilinear fibres: p-version layerwise approach. *Composite Structures*, 118:74–85, 2014.

[77] Saleh Yazdani, Pedro Ribeiro, and Jose Dias Rodrigues. A p-version layerwise model for large deflection of composite plates with curvilinear fibres. *Composite Structures*, 108:181–190, 2014.